Available online at www.sciencedirect.com
SCIENCE DIRECT®
Journal of volcanology and geothermal research
ELSEVIER
Journal of Volcanology and Geothermal Research 121 (2003) 15–63
www.elsevier.com/locate/jvolgeores

# Interpretation and utility of infrasonic records from erupting volcanoes

J.B. Johnson [a,*], R.C. Aster [b], M.C. Ruiz [c], S.D. Malone [a], P.J. McChesney [a], J.M. Lees [d], P.R. Kyle [b]

[a] *Geophysics Program, University of Washington, Seattle, WA, USA*
[b] *Department of Earth and Environmental Sciences, New Mexico Institute of Mining and Technology, Socorro, NM, USA*
[c] *Instituto Geofisico, Escuela Politecnica Nacional, Quito, Ecuador*
[d] *Department of Geological Sciences, University of North Carolina, Chapel Hill, NC, USA*

Received 22 October 2001; received in revised form 29 April 2002; accepted 29 April 2002

**Abstract**

In the most basic seismo–acoustic studies at volcanoes, infrasound monitoring enables differentiation between sub-surface seismicity and the seismicity associated with gas release. Under optimal conditions, complicated degassing signals can be understood, relative explosion size can be assessed, and variable seismo–acoustic energy partitioning can be interpreted. The extent to which these points may be investigated depends upon the quality of the infrasonic records (a function of background wind noise, microphone sensitivity, and microphone array geometry) and the type of activity generated by the volcano (frequency of explosions, bandwidth of the signals, and coupling efficiency of the explosion to elastic energy). To illustrate the features, benefits, and limitations of infrasonic recordings at volcanoes, we showcase acoustic and seismic records from five volcanoes characterized by explosive degassing. These five volcanoes (Erebus in Antarctica, Karymsky in Russia, and Sangay, Tungurahua, and Pichincha in Ecuador) were the focus of seismo–acoustic experiments between 1997 and 2000. Each case study provides background information about the volcanic activity, an overview of visual observations during the period of monitoring, and examples of seismo–acoustic data. We discuss the benefits and utility of the infrasound study at each respective volcano. Finally, we compare the infrasound records and eruptive activity from these volcanoes with other volcanoes that have been the focus of previous seismo–acoustic experiments.


*Keywords:* volcano monitoring; volcanic infrasound; volcano seismology; degassing mechanisms

## 1. Introduction

We present an overview of seismo–acoustic experiments at five active volcanoes with different eruptive styles. Activity at these sites ranges from low and medium viscosity Strombolian explosions to Vulcanian activity and volcanism associated with an active dome. The field sites are

* Corresponding author. Present address: Hawaii Institute of Geophysics and Planetology, University of Hawaii, Manoa, HI, USA. Tel.: +1-808-956-3149; Fax: +1-808-956-6322.
*E-mail addresses:* jbj@higp.hawaii.edu (J.B. Johnson), aster@nmt.edu (R.C. Aster), mruiz@dutchman.nmt.edu (M.C. Ruiz), steve@geophys.washington.edu (S.D. Malone), pmc@geophys.washington.edu (P.J. McChesney), jonathan_lees@unc.edu (J.M. Lees), kyle@nmt.edu (P.R. Kyle).

0377-0273/02/$ – see front matter 
PII: S0377-0273(02)00409-2

introduced in the order of their relative eruptive vigor, beginning with Erebus Volcano, progressing through Karymsky, Sangay, and Tungurahua, and concluding with Pichincha Volcano. We discuss each volcano with three short sections summarizing: (1) the volcano history and field experiment, (2) a data overview, and (3) the utility of infrasonic monitoring at that particular site. For each volcano, we provide examples of seismo–acoustic signals, associated frequency spectra, and observations of the associated volcanic degassing. Though we introduce various models for volcanic degassing, detailed analysis and interpretation of the seismo–acoustic signals are beyond the scope of this paper. In general, data are left in a raw, unfiltered format and normalized acoustic

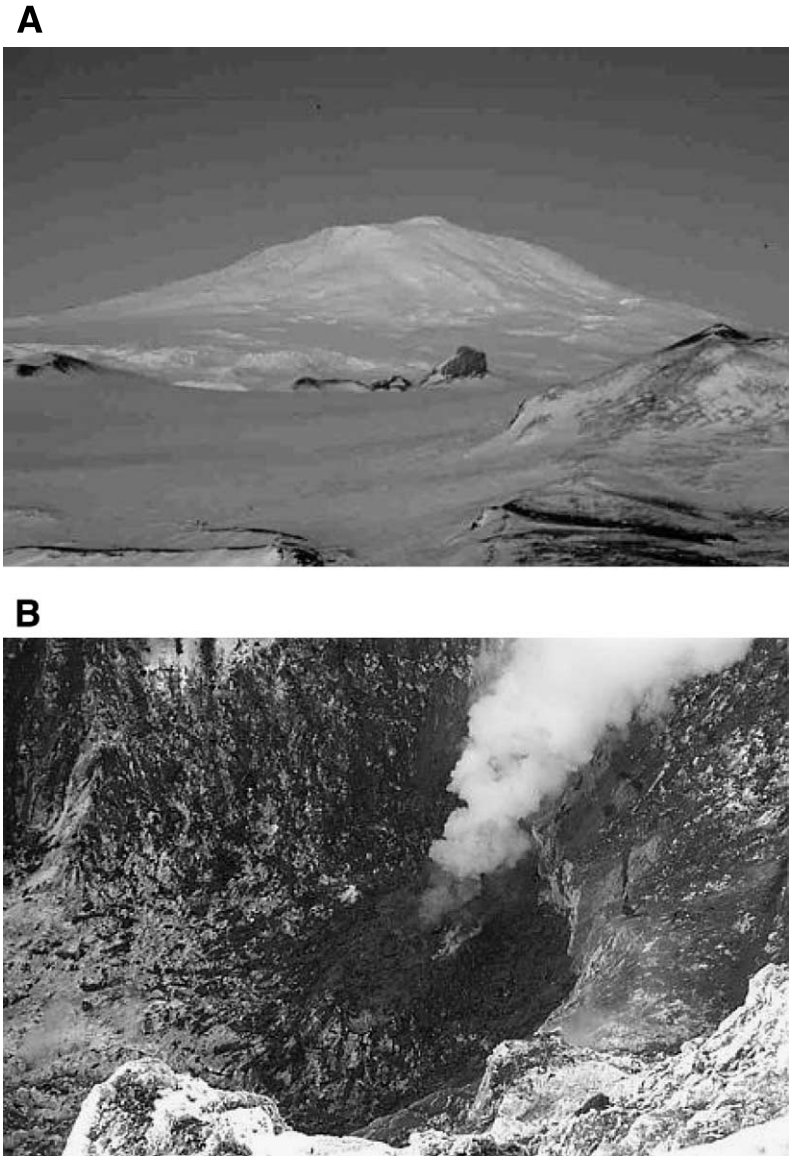


Fig. 1. Erebus Volcano. (A) View from McMurdo towards Erebus 40 km to the north. (B) Erebus lava lake in December 1999 as seen from the crater rim ~200 m above the lava lake. Photos courtesy of B. Johns.

pressure traces and raw velocity seismograms are used nearly exclusively. Specifications of the microphones used in these experiments are included in an Appendix. A summary of the fundamentals of volcanic infrasound generation and propagation is provided in an accompanying paper (Johnson, in press).

## 2. Erebus Volcano (1999–2000)

### 2.1. Background

Erebus is a 3700-m shield volcano located on Ross Island, Antarctica (Fig. 1). Since its first sighting in 1841 Erebus has been considered to be in a continuous open vent state, manifesting a permanently convecting lava lake in the summit crater [Kyle et al., 1982). This lava lake constitutes a skylight into an unroofed shallow magma chamber through which gas can escape without a corresponding flux of magma (Rowe et al., 2000). The lava lake composition is phonolite, a relatively rare, high-temperature, highly alkalic magma with basic to intermediate silica content and a viscosity that is similar to or somewhat less than average basaltic magma (Dibble et al., 1984). During the period of our study, from November 1999 through January 2000, eruptive activity was characterized by explosive gas bubble ruptures which were powerful enough to eject some magma fragments approximately 400 m vertically up and out over the crater rim (Bjorn Johns, pers. commun., 2000). These bubble ruptures originated from a 10-m radius skylight in the floor of the crater.

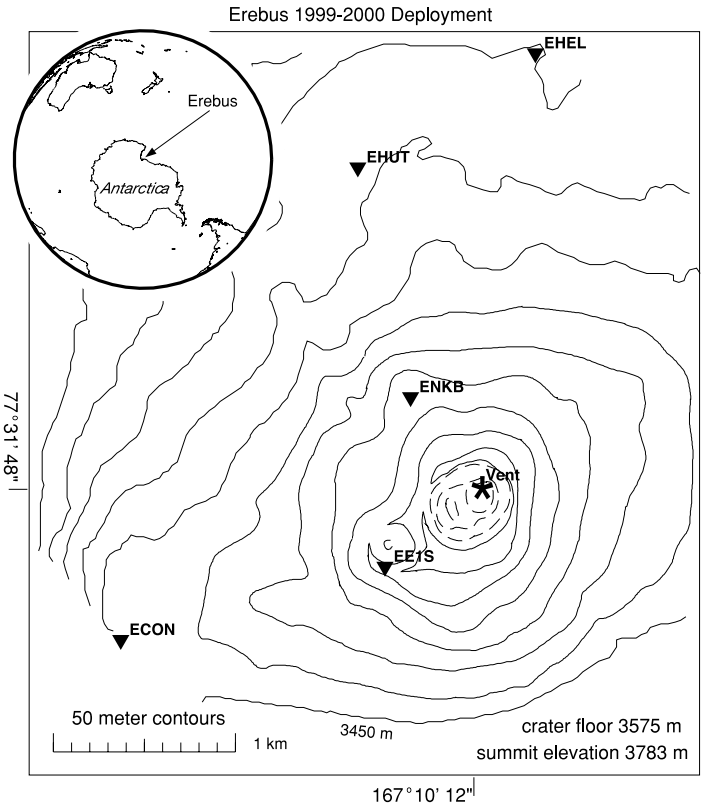


Fig. 2. Erebus Volcano, 1999–2000 deployment map. Each of the five stations was equipped with a broadband seismometer and microphone(s). Stations EE1S and EHUT were equipped with two microphones each for calibration purposes.

During the 1999–2000 field season we deployed five stations equipped with McChesney 4-element microphones. Broadband seismometers (CMG3ESP and CMG-3T) were also installed at these five sites located 670–2450 m from the lava lake (Fig. 2). Recording was continuous at 40 samples per second on portable PASSCAL Reftek A-08 dataloggers. The nearest seismo–acoustic station to the vent (EE1S) was co-located with a Dibble pressure transducer microphone and a station 1900 m from the vent (EHUT) was also equipped with a Larson–Davis free-field precision microphone. The temporary network recorded 2–5 explosions each day for nearly two months.

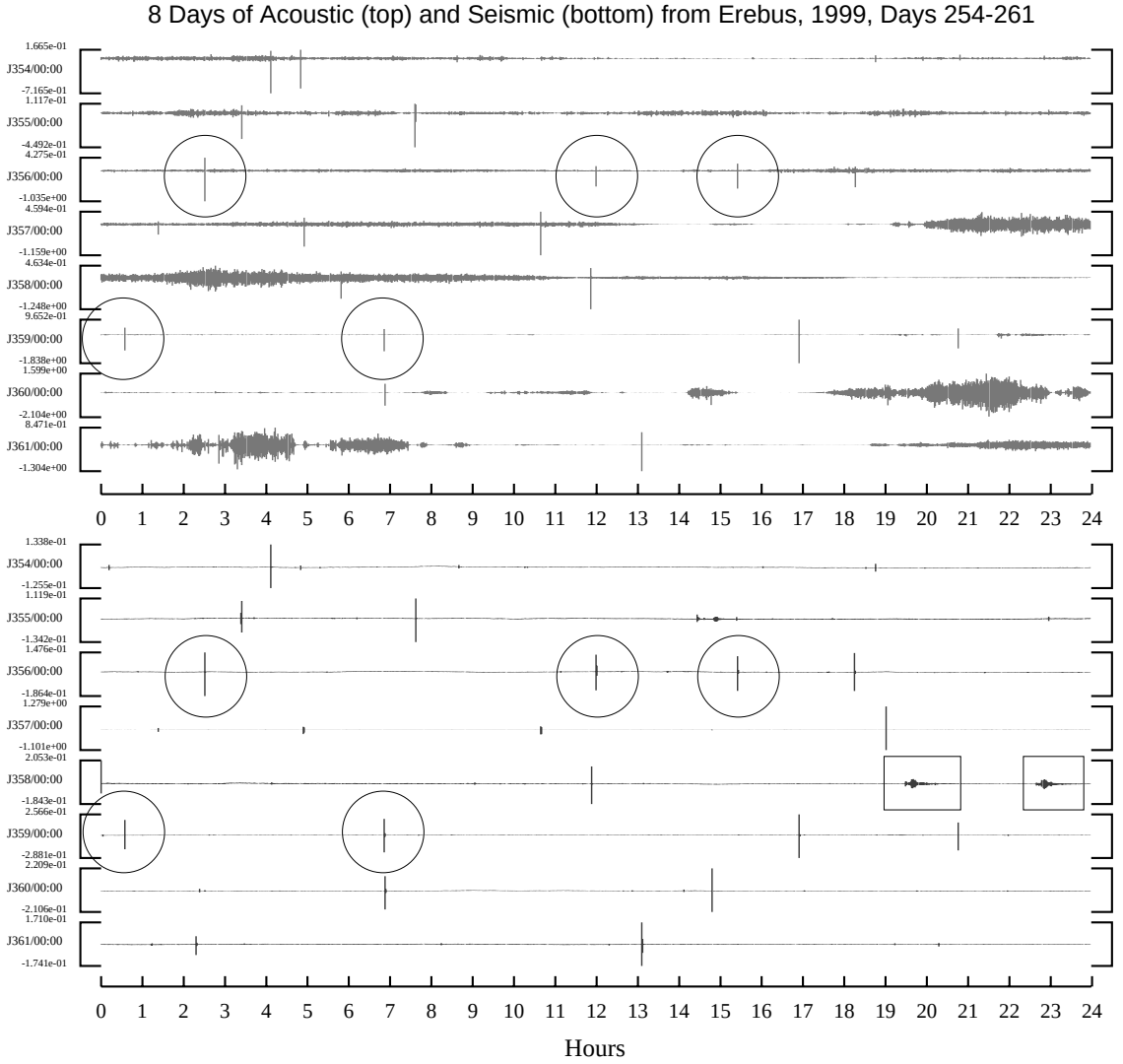


Fig. 3. Erebus 8-day acoustogram and seismogram. Eight days of continual data (day 254–261, 1999) recorded at station EHUT (acoustic normalized pressure; top) and EE1S (seismic normalized velocity; bottom). Acoustic data are displayed from EHUT rather than EE1S because many acoustic signals are clipped at EE1S. Selected events (indicated by boxes) are teleseisms. Long-duration acoustic tremor signals in the top panel represent periods of high wind noise. Circled events correspond to the explosions displayed in Fig. 4.

### 2.2. Data overview

Although periods of windy weather were responsible for high noise levels in some infrasonic pressure records (see long-duration 'acoustic tremor' signals in Fig. 3), about 90% of the explosions at Erebus were recorded clearly. This high recovery rate may be attributed to the wind-filtering benefits of the overlying snow, spatial filtering of the 4-element microphones (see Appendix), proximity of the microphones to the explosion source, and the relatively high signal strength of Erebus infrasound. All recorded acoustic signals from Erebus in 1999–2000 are very simple explosion events, beginning compressively and impulsively and possessing minimal coda ($\sim$5 s). Consistent lag times between seismic and acoustic phases and self-similarity of seismic and acoustic wavelets for different explosions (Fig. 4), indicate a repeatable source. These explosion signals are similar in appearance to the simple infrasonic pulses recorded at Stromboli Volcano (Vergniolle et al., 1996). At both Stromboli and Erebus, large bubbles (radius greater than 1 m) have been observed rising to the surface of a fluid magma and forming blisters before bursting.

Travel time differences between acoustic and seismic phases are dependent upon epicentral distance (Fig. 5). Because Erebus acoustic arrivals are so impulsive, apparent acoustic velocities can be determined easily for infrasound recorded across the array. For our suite of explosions, infrasonic apparent velocities are $315 \pm 5$ m/s, corresponding to atmospheric temperatures ranging from $-34$ to $-23°$ Celsius (typical conditions at Erebus). Seismic arrivals in the short-period band are extremely emergent with an estimated first arrival apparent velocity of $3300 \pm 300$ m/s. This velocity is somewhat slower than the 4070-m/s P-wave velocity that was determined by Dibble et al. (1994) for explosions at Erebus. Nevertheless, with the resolution afforded by our seismo–acoustic array at Erebus in 1999–2000, it appears that the onset of both acoustic and high-frequency seismic signals emanate from a synchronous source at the vent. Although there is no evidence of precursory high-frequency seismicity prior to bubble rupture, broadband records show very long-period (VLP) signals that begin approximately 4 s before the explosion (middle panel of Fig. 4). This VLP signal, with a dominant period of 7 s, reflects conduit resonance or inertial reequilibration of the lava lake associated with the upward transit of a gas slug (Rowe et al., 2000).

Low acoustic phase velocities enable the accurate location of explosion sources through examination of arrival times across the array of microphones. Relative acoustic arrival times are determined through a waveform cross-correlation algorithm which is checked by an analyst. Interpreted explosion epicenters (Fig. 6) correspond to the lowest total mean squared distance residuals (determined by a grid search with 2-m spacing, equal weighting for all five stations, and a homogenous 315-m/s atmospheric velocity structure). Erebus explosion epicenters located in this manner have a spatial standard deviation of 9 m. During the 1999–2000 field season, the 10-m radius lava lake had a fixed position, implying that much interpreted source location variability is an artifact of changeable atmospheric temperature or wind structure.

Regardless of explosion size, the self-similarity of acoustic explosion signals lasts for more than 5 s (bottom panel of Fig. 4). Portions of this acoustic 'coda' may be attributed to artifacts of atmospheric propagation. A second compressional pulse (marked by an arrow in the Fig. 4 overlay) follows the original acoustic pulse by about 1.7 s, suggesting an 'echo' off the crater wall about 260 m from the lava lake. This dimension is compatible with the size of the 400-m-radius Erebus crater.

The intensity of Erebus explosions can be investigated by analyzing reduced seismic body wave displacements ($D_R$ = Displacement amplitude $\times$ Radial distance/$2\sqrt{2}$ (Aki and Koyanagi, 1981)) and reduced acoustic pressures ($P_R$ = Excess pressure $\times$ Radial distance (Johnson, 2000)). These two parameters are measures of the peak trace amplitude taking into consideration amplitude loss due to spherical spreading. At Erebus, the size and overpressure of a ruptured bubble determines the acceleration of gas injected into the atmosphere which is proportional to the am-

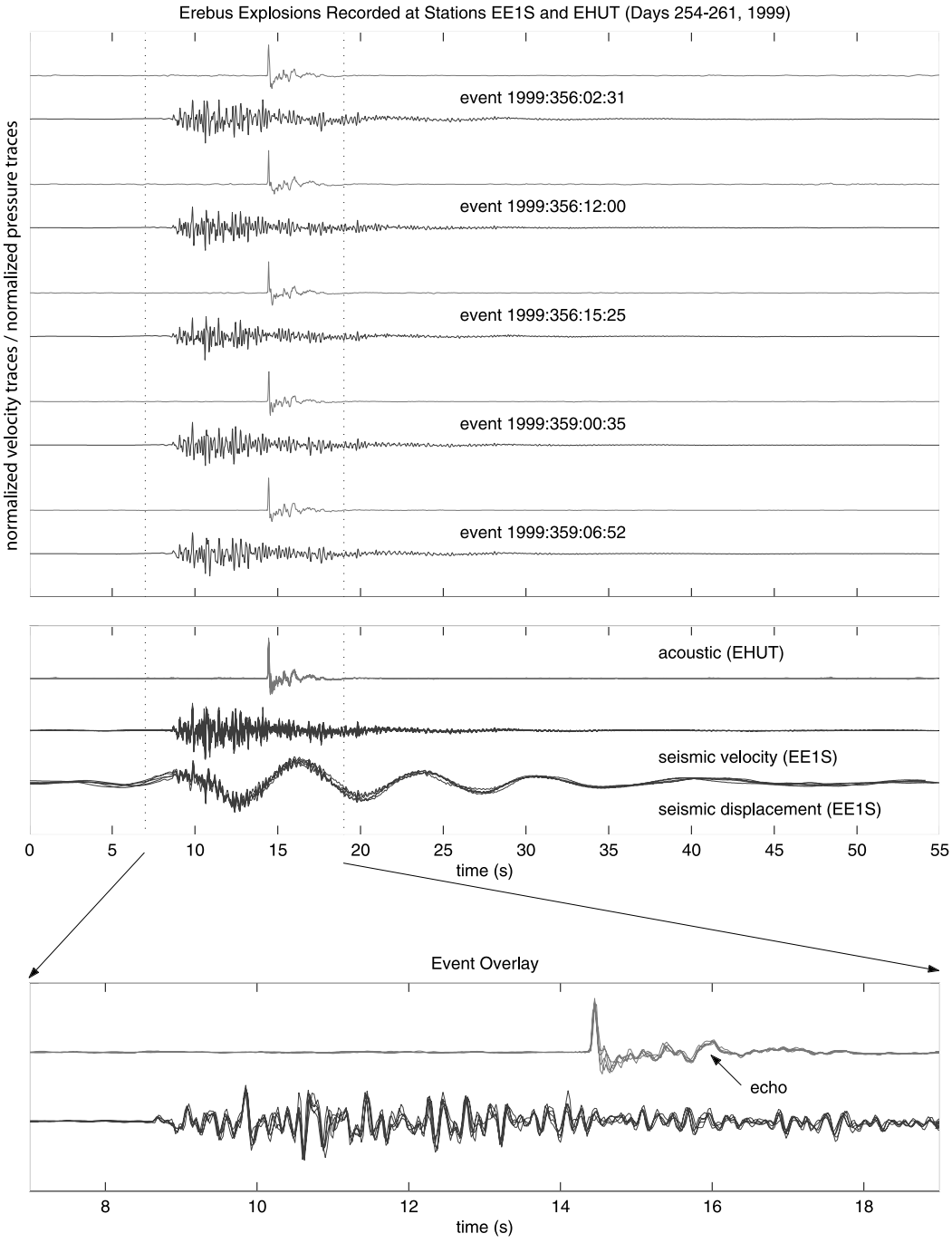


Fig. 4. Erebus explosion examples; selected normalized explosion waveforms from Fig. 3 (indicated by circles). An overlay of the five events is provided in the bottom two panels. Acoustic and seismic traces, including displacement waveforms (bottom trace in middle panel), show excellent self-similarity for different explosions. The arrow in the lowermost panel indicates a possible acoustic echo off the Erebus crater wall.

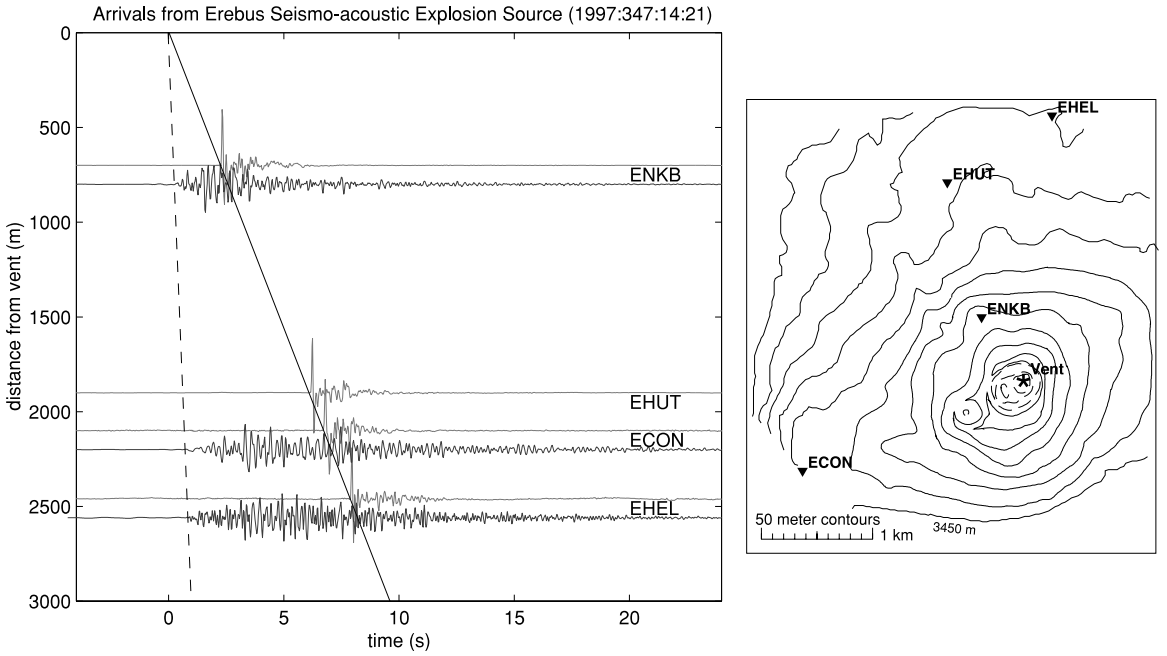


Fig. 5. Erebus explosion seismo–acoustic arrivals. Erebus explosion recorded at several stations reveals phase velocities for acoustic and seismic waves. Seismic velocity traces are filtered above 2 s to remove precursory VLP signal. Apparent acoustic velocity is 313 m/s and apparent seismic velocity of the first arrivals is ~3300 m/s. Short-period body wave velocity is difficult to accurately determine due to the emergent nature of the seismic waveforms.

plitude of the infrasonic pulse (Johnson, 2000). In theory, explosion size should also be correlated with seismic displacement amplitude because it produces a corresponding thrust force exerted on the volcano (Kanamori and Given, 1982; Brodsky et al., 1999). At Erebus we do observe a consistent relationship between maximum excess acoustic pressure and maximum seismic displacement that appears independent of explosion size (Fig. 7). This is further evidence of a repeatable explosion mechanism. However, at many other volcanoes, notably Langila (Mori et al., 1989), Arenal (Hagerty et al., 2000), Unzen (Yamasato, 1998), and Karymsky (Johnson and Lees, 2000), energy partitioning between seismic and acoustic phases is inconsistent. Scatter in seismo–acoustic energy partitioning at these sites may be explained by variable explosion source locations within a volcanic conduit (Johnson, 2000) or by changing acoustic properties of the two-phased magma (Garces et al., 1998). During the 1999–2000 season Erebus exhibited no such scatter, indicating that all explosions originated at consistent locations within a small lava lake and probably shared consistent coupling and propagation parameters. Rowe et al. (2000) investigated seismo–acoustic amplitude ratios for Erebus explosion events between 1997 and 1998 and noted that although moderate to large explosions exhibited similar size-independent energy partitioning, a systematic decrease in seismic efficiency was apparent for the smallest explosions. This variation is attributed to impedance isolation or attenuation differences associated with the smallest, shallowest gas bursts (Rowe et al., 2000).

### 2.3. Utility of acoustic monitoring

A defining characteristic of Erebus eruptive activity is the bursting of large intact bubbles at the surface of a low-viscosity phonolitic magma lake. The relative absence of an acoustic coda in association with the explosion events is evidence for the open nature of the Erebus plumbing system. It

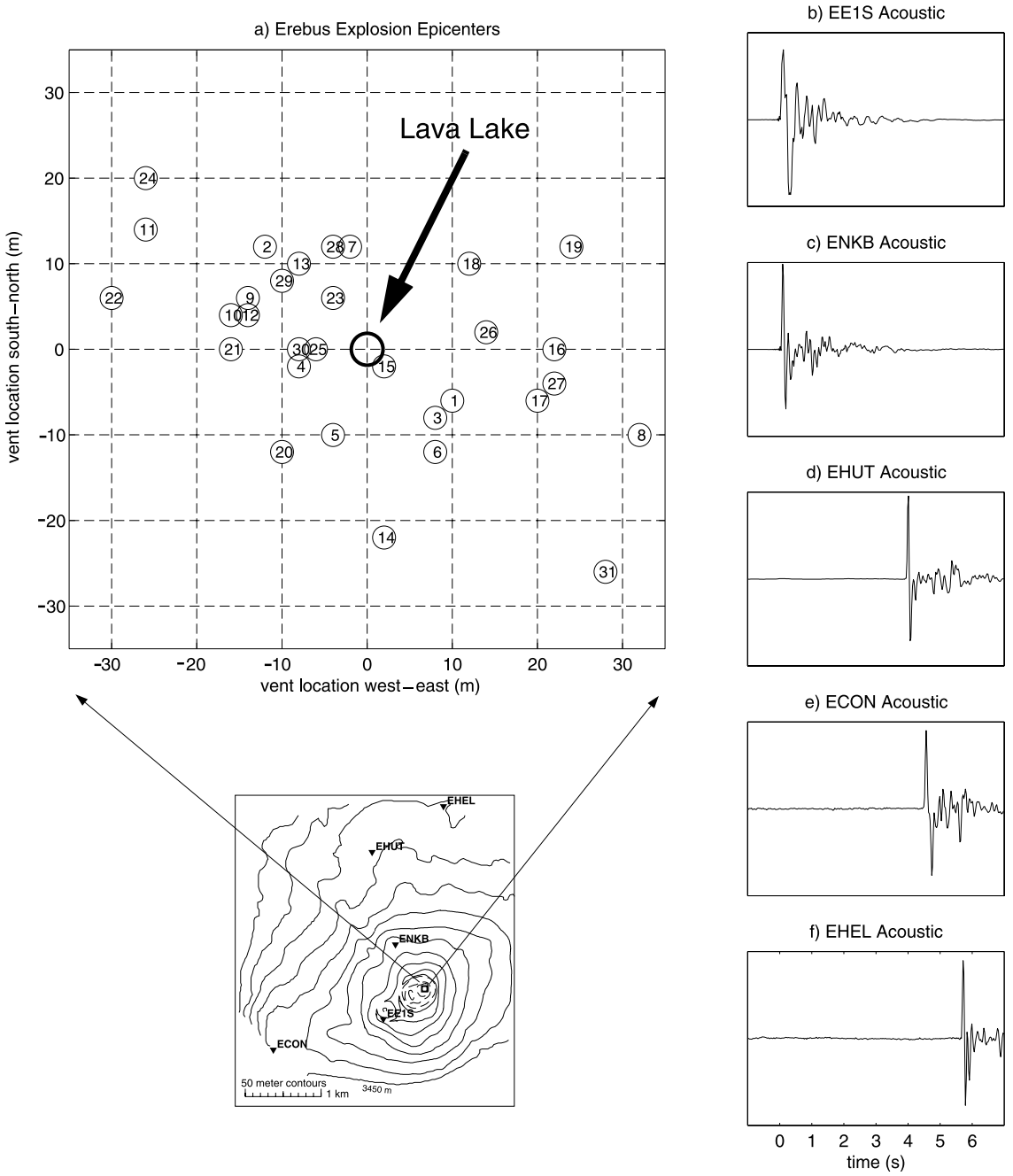


Fig. 6. Erebus vent locations. (a) Vent locations determined by grid search for a suite of 31 Erebus explosions (numbered chronologically) occurring between 1999:347:14 and 1999:362:08. (b–f) Normalized pressure traces for event No. 1 (1999:347:14:21) are shown for the five infrasound stations in the array.

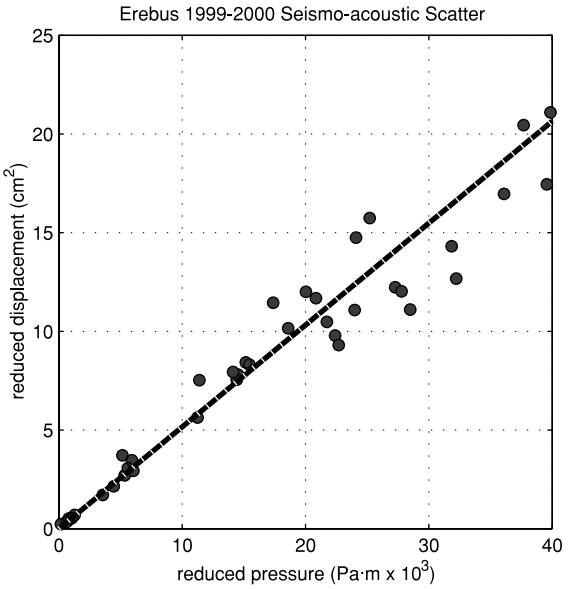


Fig. 7. Erebus seismo–acoustic scatter. Reduced pressures plotted against reduced displacements for a suite of 64 explosions reveal consistent seismo–acoustic energy partitioning at Erebus during 1999–2000.

is probable that all explosive degassing events occurring at Erebus during the 1999–2000 field season were manifested as bubble bursts at the surface of the lava lake. Variations in explosion size, as recorded on both seismic and acoustic channels, reflect the volume of gas released and/or gas overpressure of the bursting bubbles.

Erebus serves as a low-viscosity end member for explosive volcanic degassing. Bubbles are able to rise relatively unhindered through the conduit until they reach the surface of the lava lake, generating relatively simple, short, repeatable explosions. Our study at Erebus provided good azimuthal and radial coverage of the acoustic wavefield by well-calibrated microphones which enable good constraints of the explosion source-pressure time histories. The influences of weather upon inferred vent location and acoustic pressure amplitudes can thus be studied in detail. Microphone arrays such as the one deployed at Erebus are especially valuable for filtering out weather variations and recovering true explosion source parameters.

## 3. Karymsky (1997, 1998, 1999)

### 3.1. Background

Karymsky Volcano (Fig. 8) is a 1540-m andesitic cone located in the central portion of Kamchatka's main active arc. Its most recent eruptive phase began in January, 1996 after 14 years of quiescence (Gordeev et al., 1997). Though the eruption onset was initially characterized as Vulcanian behavior, activity evolved to a Strombolian behavior by the summer of 1996. Between 1996 and 1999, Karymsky produced discrete Strombolian explosions, with a frequency ranging from 5 to 20 events per hour. A flux of magmatic material in the form of bombs and block lava flows accompanied the Strombolian activity. Periods of relative explosive vigor, with andesitic block lava flows extending over a kilometer from the summit vent, occurred during the summers of 1996 and 1998. Explosion frequency and intensity began diminishing in 1999 and as of October, 2001, Karymsky is erupting intermittently (Evgenii Gordeev, pers. commun., 2001).

Our three field trips to Karymsky (August, 1997, September, 1998, and September, 1999) provided three high-quality datasets of acoustic and seismic recordings. In all experiments, we deployed PASSCAL Reftek A-07 and A-08 dataloggers on the lower flanks of the volcano, 1500–5000 m from the summit vent. Most stations were equipped with 3-component broadband seismometers and either one or two microphones. Recording sample rates were either 100 or 125 samples per second.

In the 1997 field season (Fig. 9a), both a Ripepe microphone and a Ramey differential pressure transducer microphone were co-located with a CMG 40-T broadband seismometer that operated for three days at station Kar1 (1620 m from the active vent). During the study, discrete explosive events occurred on average 10 times each hour. In the 1998 field season (Fig. 9b), eight electret condenser microphones (one Larson–Davis free-field precision microphone, four Ripepe microphones, and three Venema microphones) were deployed at epicentral distances ranging from 1500 to 3000 m. Each microphone was co-located with either a

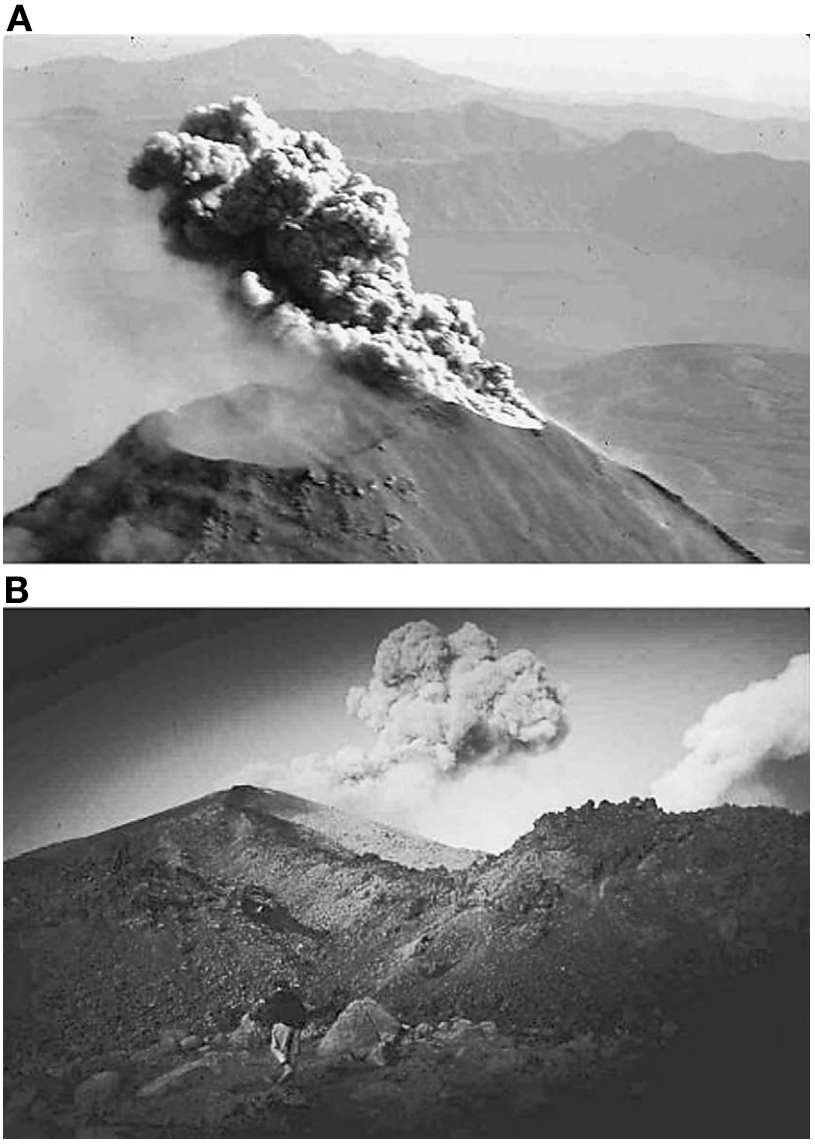


Fig. 8. Karymsky Volcanoe. (A) View of summit crater and explosive gas emissions in 1998. (B) View from the base of the active block lava flow of 1998 (~1300 m from vent). Photos courtesy of L. Clabaugh.

CMG 40-T or a short-period (1-s) seismometer. The experiment lasted nine days with individual campaigns of one or two days. Campaign geometries included a linear array aligned radially with the vent, an array with azimuthally distinct station locations, and calibration tests in which all microphones were co-located at a single site. In 1998, explosive events occurred on average 15 times each hour. During the 1999 field season (Fig. 9c), eight electret condenser microphones (one Larson–Davis free-field precision microphone, one Venema microphone, and six McChesney microphones) were deployed for four days at five stations with epicentral distances ranging from 1500 to 5000 m. Several stations housed multiple microphones for calibration and

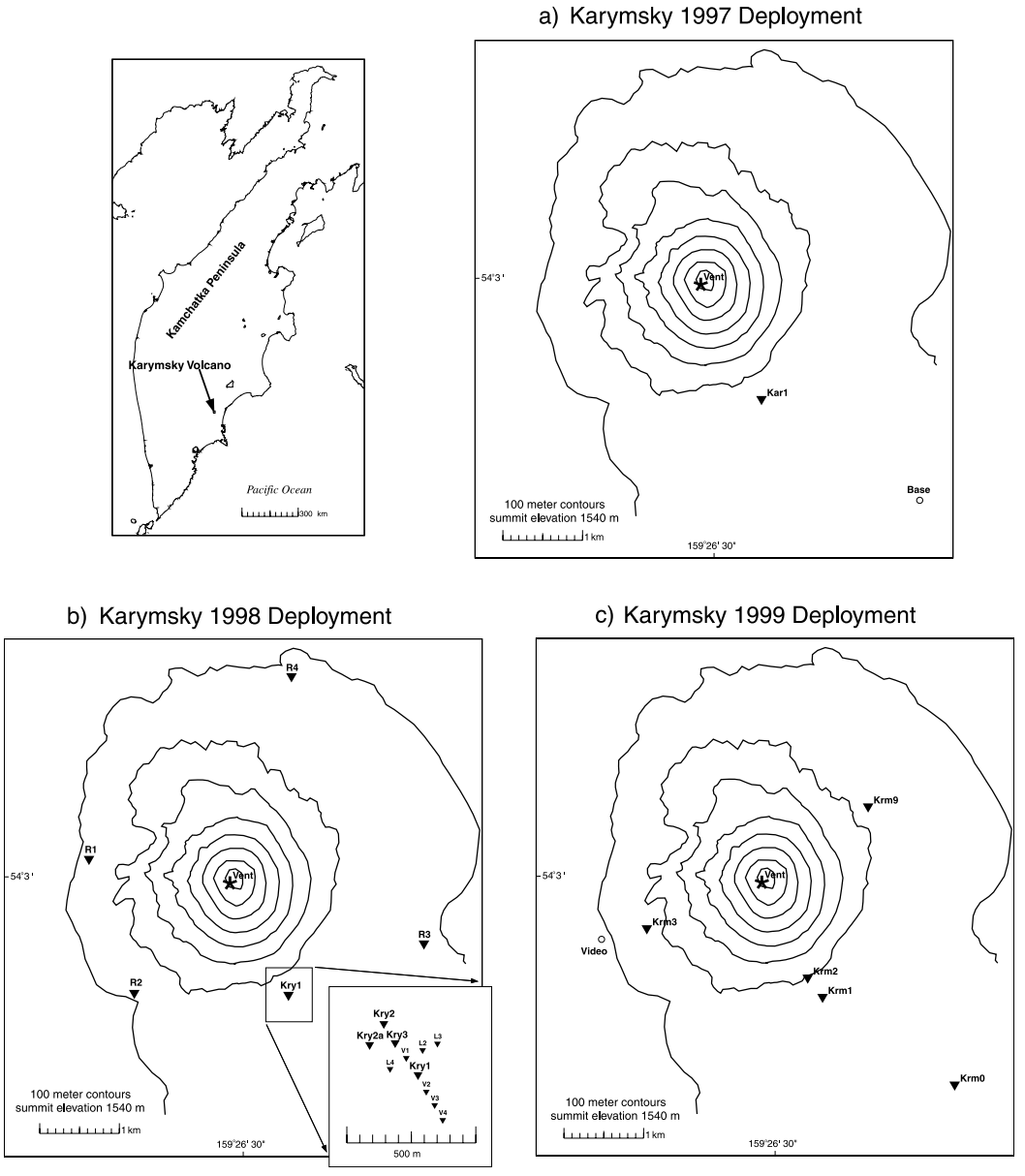


Fig. 9. Map of Karymsky stations. All marked stations housed at least one microphone and a seismometer. (a) Karymsky 1997 deployment map. (b) Karymsky 1998 deployment map. Stations L1-4, V1-4, and R1-4 were each part of individual campaigns lasting one or two days. Stations Kry1-3 were fixed for the duration of the experiment. (c) Karymsky 1999 deployment map.

wind filtering purposes (see Appendix). In this experiment, three CMG 40-T and two STS-2 broadband seismometers were co-located with the microphones. On average, explosive events occurred 8 times each hour.

### 3.2. Data overview

During periods of low acoustic noise (low wind), virtually all Karymksy seismic signals are associated with acoustic signals (Figs. 10A–C and

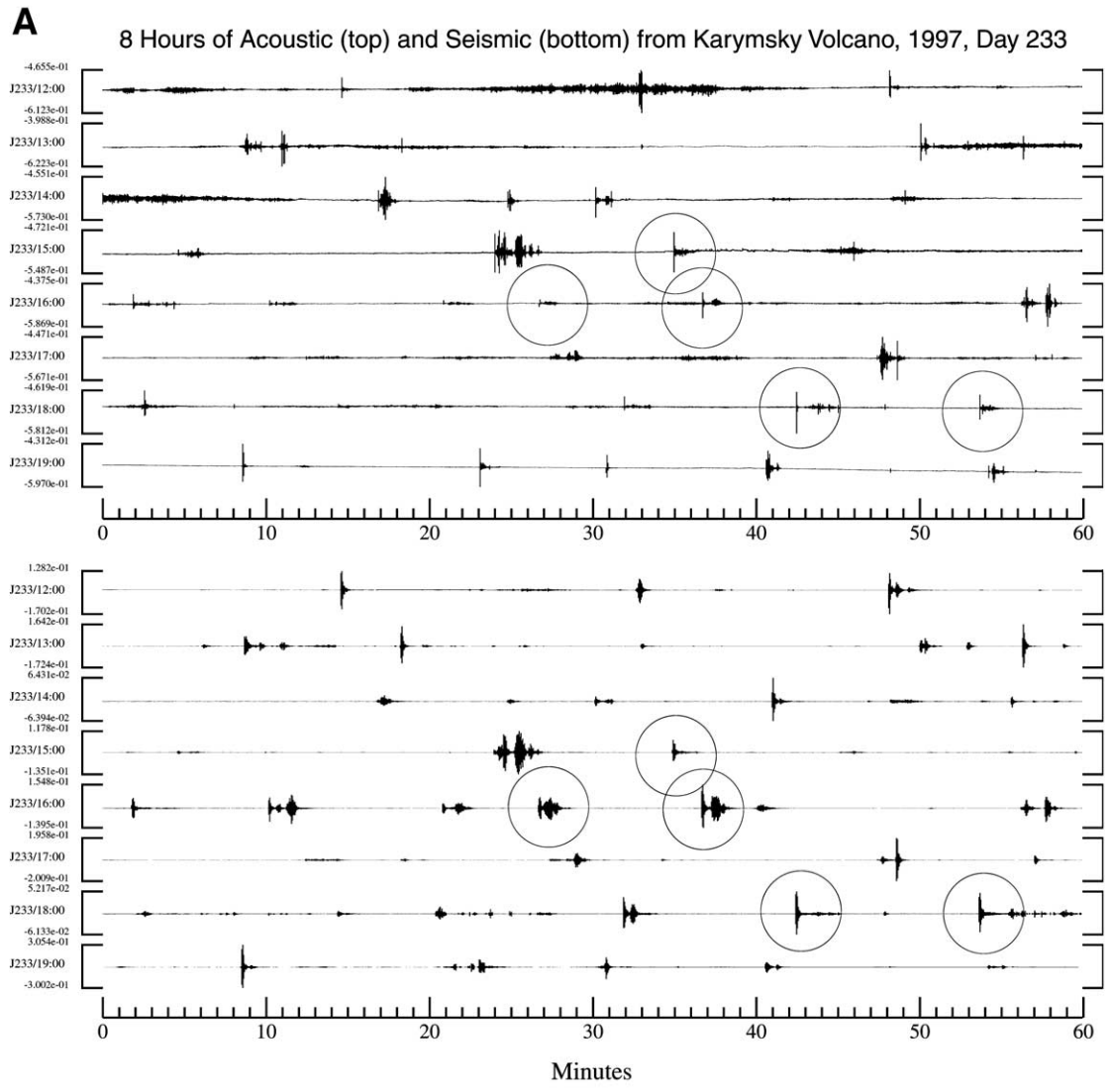


Fig. 10. Karymsky 8-h acoustogram and seismogram. (A) Eight hours of activity recorded at station Kar1, day 233, 1997. Acoustic signals are recorded with a Ripepe microphone (top) and seismic signals are recorded with a CMG-40T broadband seismometer (bottom). Circled events correspond to the explosions displayed in Fig. 11A. (B) Eight hours of activity recorded at station Kry1, day 248, 1999. Acoustic signals are recorded with Larson–Davis microphone (top) and seismic signals are recorded with CMG-40T broadband seismometers (bottom). Circled events correspond to the explosions displayed in Fig. 11B. (C) Eight hours of activity recorded at station Krm1, day 251, 1999. Acoustic signals are recorded with a McChesney microphone (top) and seismic signals are recorded with CMG-40T broadband seismometers (bottom). Wind noise appears as tremor throughout much of the acoustogram. Circled events correspond to the explosions displayed in Fig. 11C.

11A–C). Wind noise is a persistent problem in all three Karymsky datasets that partially obscures acoustic signals in about 50% of the explosions (examples of wind noise are evident in Fig. 10C). Wind typically appears as a broadband, tremor-like signal lasting tens of seconds to hours that tends to be more prominent during daytime recording. Fortunately, the abundance and re-

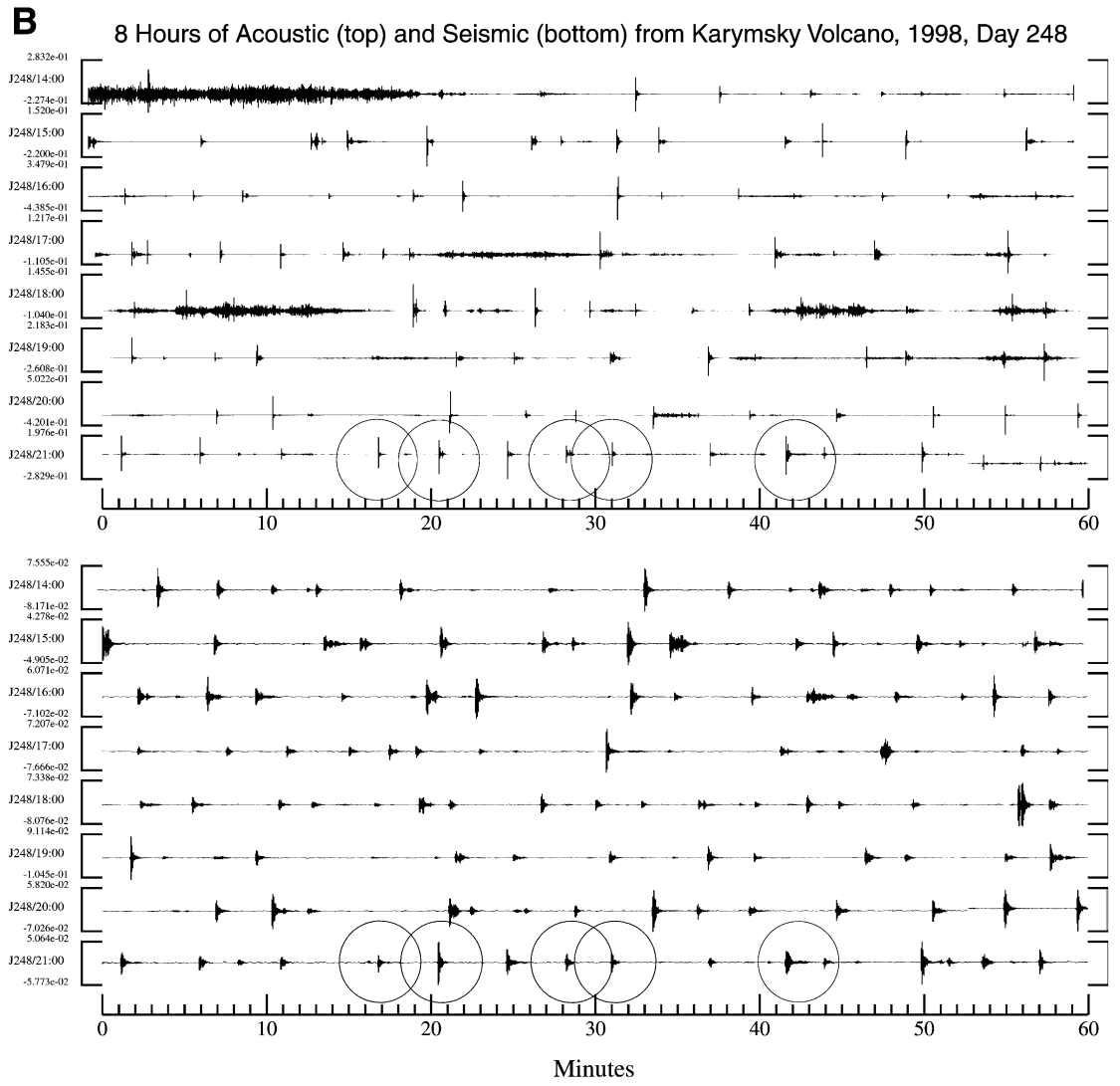


Fig. 10 (*Continued*).

peatability of explosions at Karymsky compensate for periods of time when the acoustic data are of poor quality.

Karymsky explosion onsets are nearly always characterized by rapid gas and/or ballistic emission, followed by gas effusion which tapers gradually during the course of several minutes. Discrete explosions are separated by quiescent intervals of several minutes during which degassing is not visibly evident. Incandescence is apparent only at night, most commonly at the onset of an explosion.

For nearly all Karymsky explosions, the event onset is an impulsive compressional acoustic pulse which follows an emergent seismic signal by a consistent, fixed time that is dependent upon the distance between the vent and recording site (Fig. 12). The travel time difference between the first seismic arrivals and first acoustic arrivals is roughly equal to the source-receiver distance

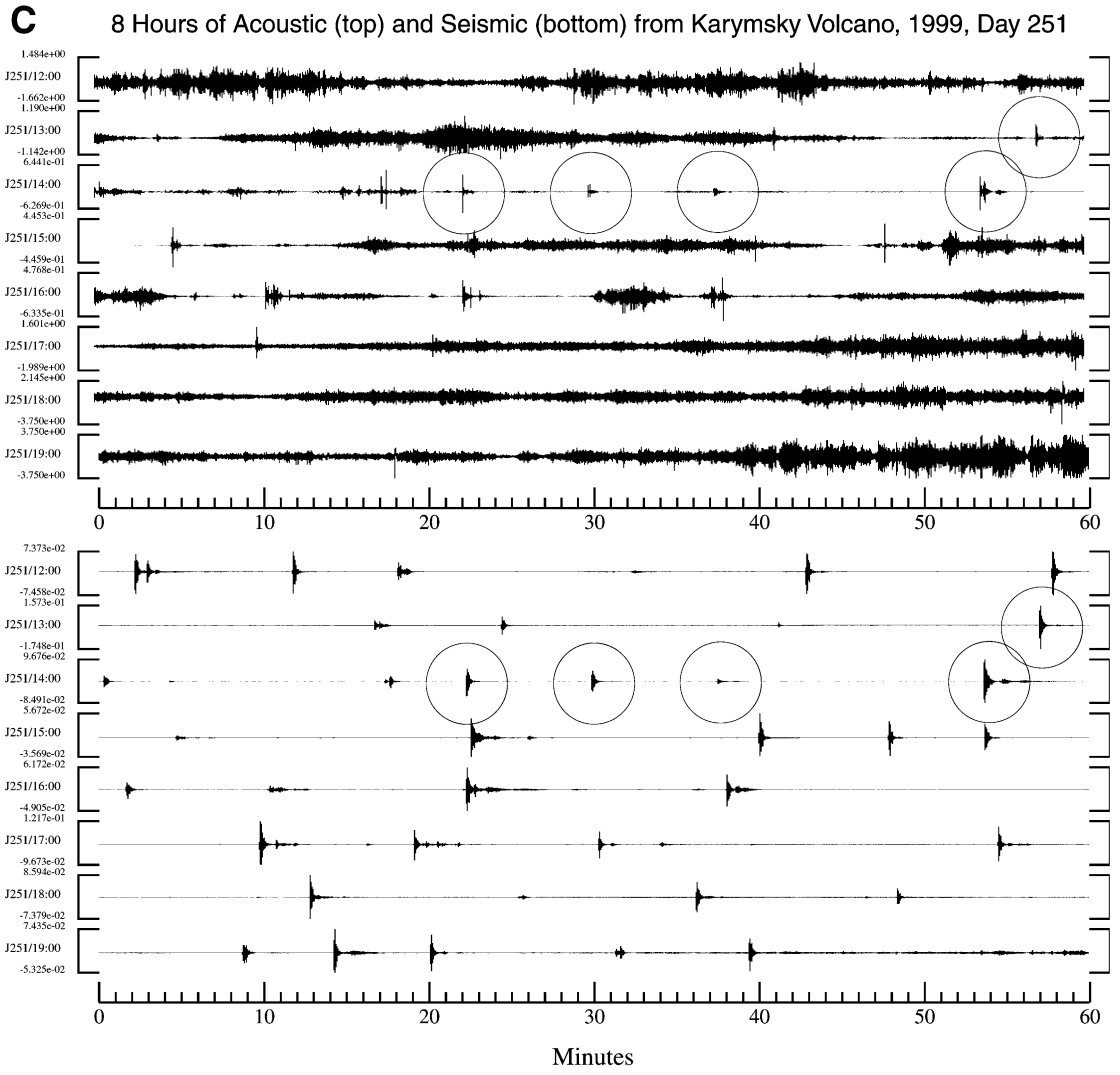


Fig. 10 (*Continued*).

times 2.1 s/km (for seismic velocities of 1200 m/s and acoustic velocities of 339 m/s). This lag time between acoustic and seismic phases varies by about 2% which can be attributed to changeable weather conditions. As at Erebus, we determine explosion epicenters by interpretation of relative acoustic arrival times at multiple stations. Fig. 13 shows a suite of inferred vent epicenters corresponding to lowest total mean square distance residuals (determined by grid search with 2-m spacing, equal weighting for three stations, and a homogenous 340 m/s atmospheric velocity structure). Since the vent is physically confined to the floor of the small summit crater (Fig. 8A), we infer that the spatial standard deviation of 6 m is largely an artifact of atmospheric variability. Epicenters that are consistently offset for periods of time lasting several hours (e.g. explosions 40–57 in Fig. 13) indicate the effects of prevailing winds during that time interval. Though the vent location determined from infrasound arrivals has errors associated with changeable atmospheric conditions, the resolution is still greatly superior to source locations calculated

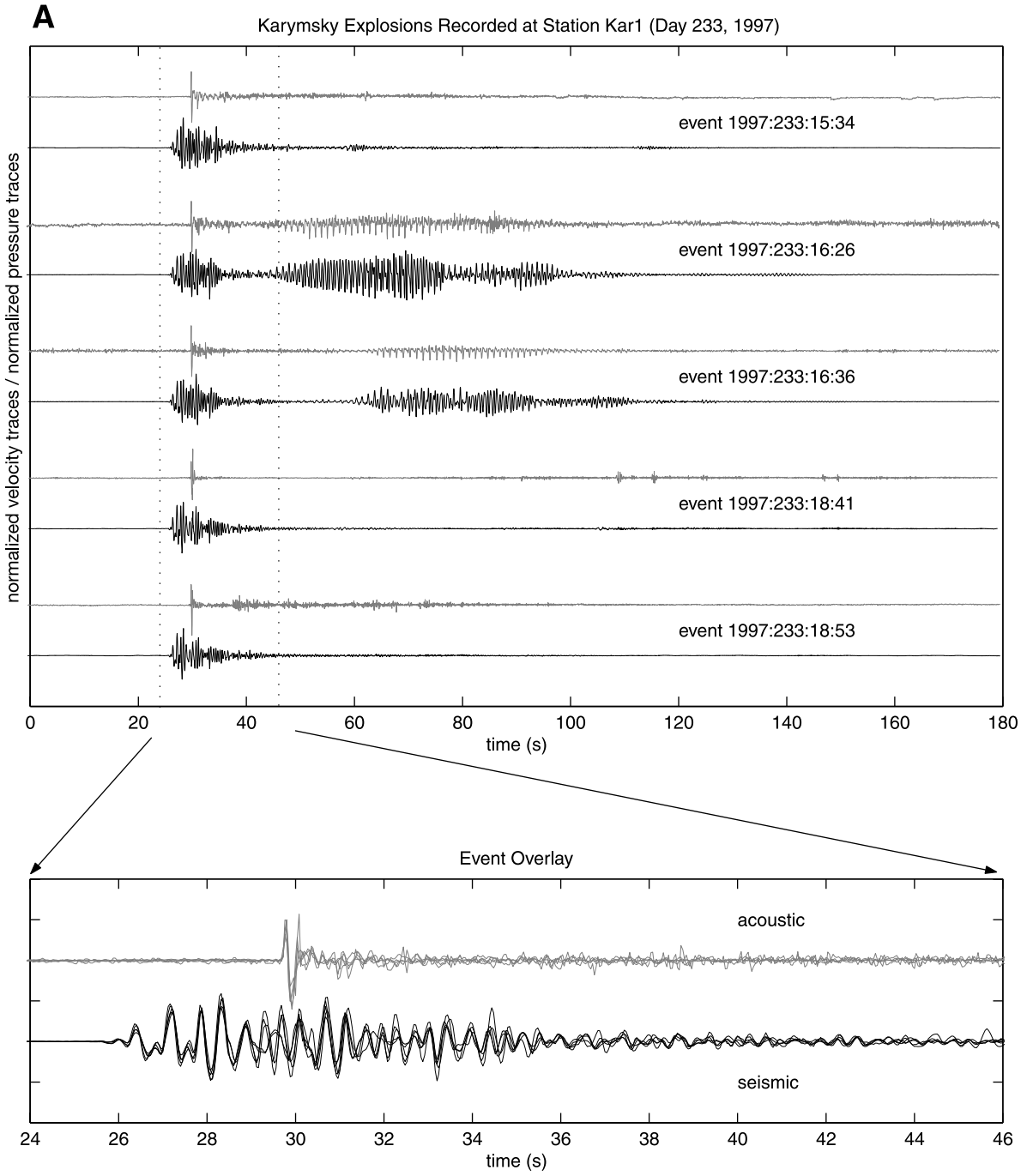


Fig. 11. Karymsky explosion examples. (A) Selected 1997 normalized explosion waveforms from Fig. 10A (indicated by circles). (B) Selected 1998 normalized explosion waveforms from Fig. 10B (indicated by circles). (C) Selected 1999 normalized explosion waveforms from Fig. 10C (indicated by circles).

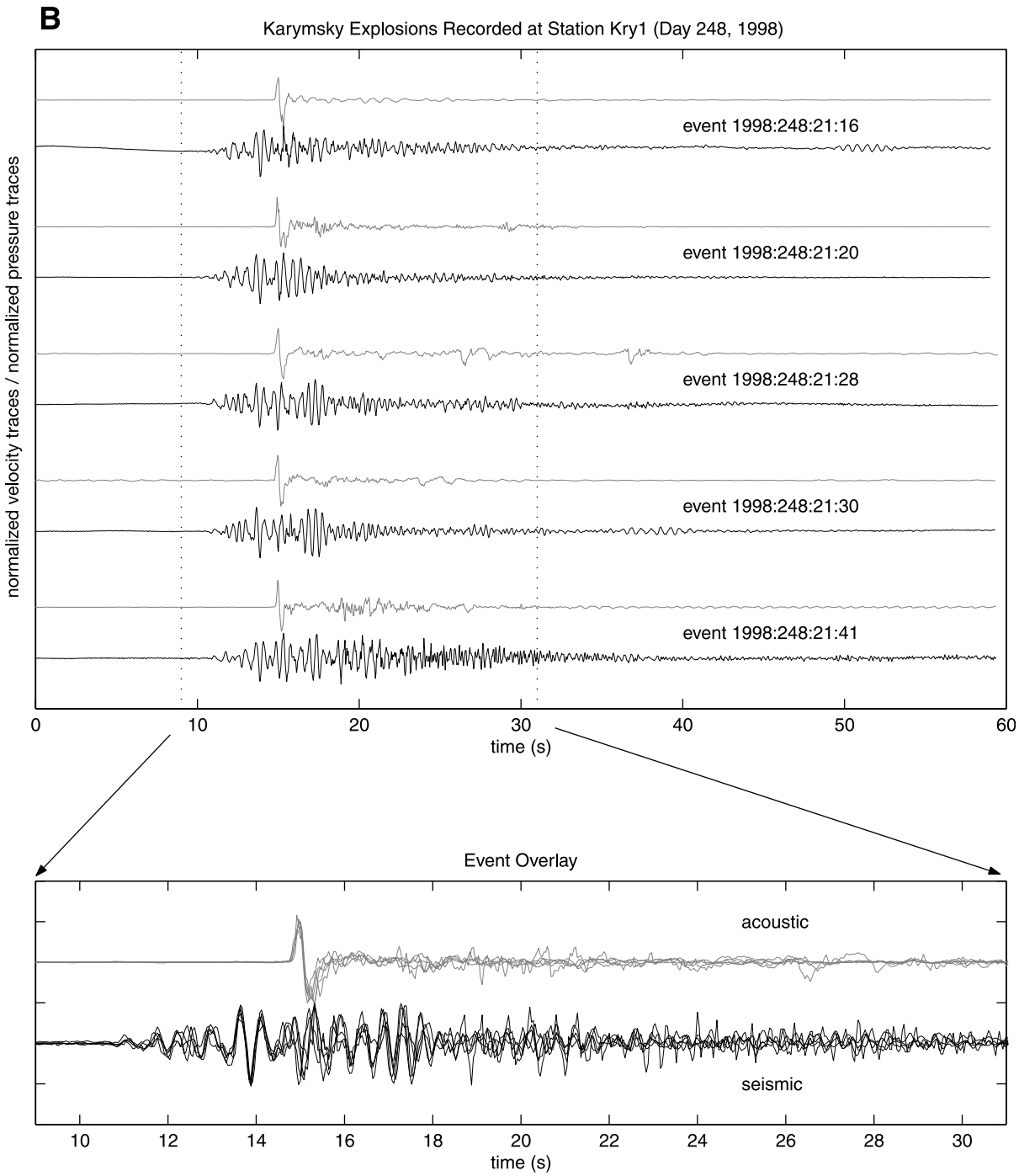


Fig. 11 (*Continued*).

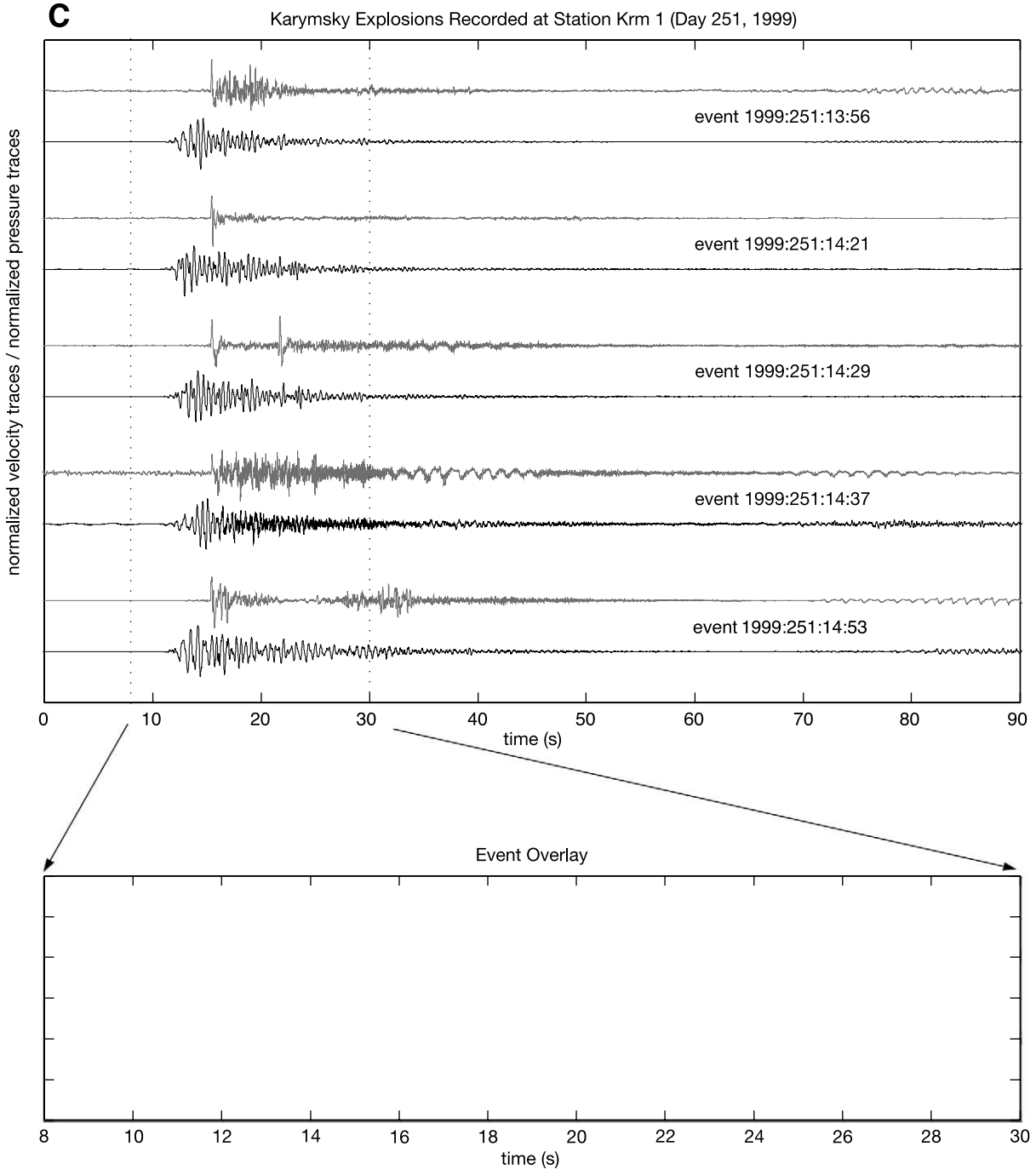


Fig. 11 (*Continued*).

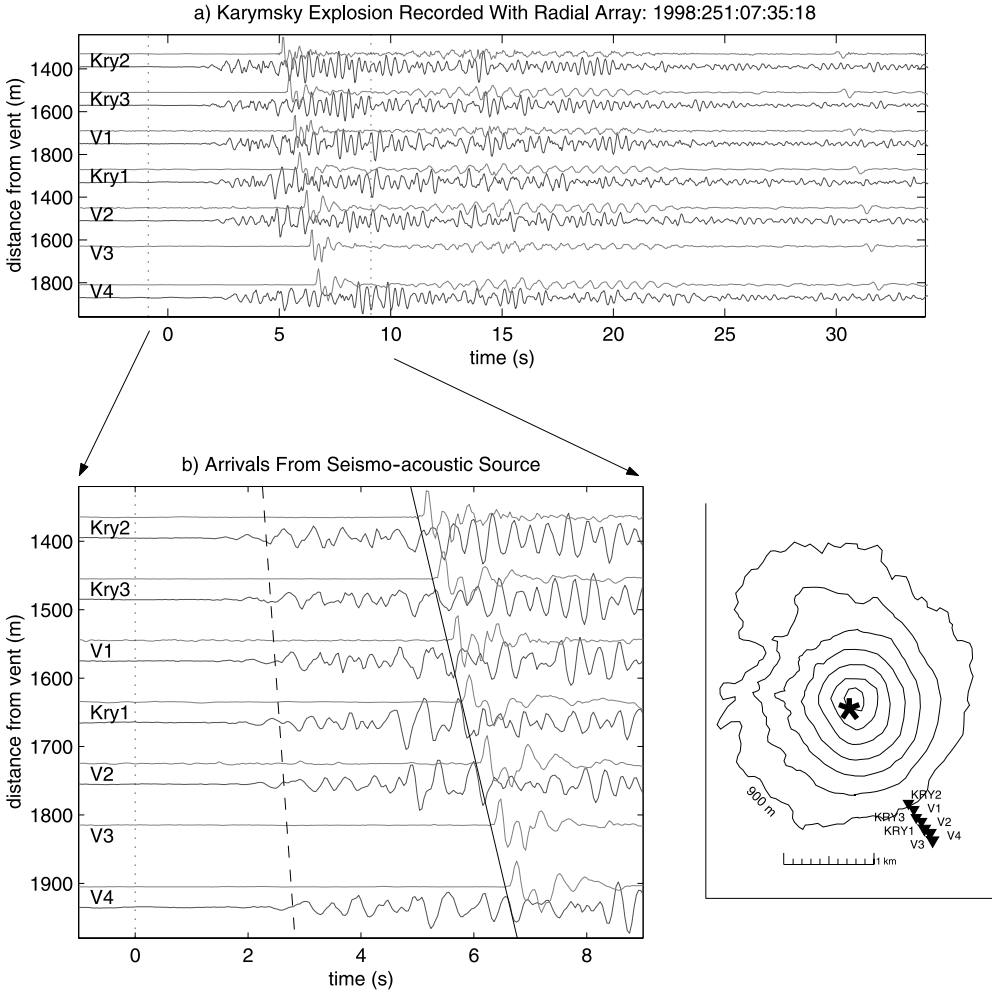


Fig. 12. Karymsky explosion seismo–acoustic arrivals. (a) Acoustic pressure traces and seismic velocity traces as recorded on the linear radial array at Karymsky in 1998. Spacing between the seven stations is 85 m with a total aperture of 510 m. (b) Enlargement with marked phases shows acoustic arrival (solid line; apparent velocity 346 m/s) and inferred seismic arrival (dashed line; apparent velocity ~1200 m/s). The seismic apparent velocity is determined through inspection of coherent 1-Hz energy (filtered signals not shown here). Both acoustic and seismic phases are plotted assuming a synchronous seismo–acoustic source at zero seconds origin time. Emergent seismic energy that is visible before the dashed line may be an indicator of a low-amplitude pre-explosion seismic source.

through the analysis of seismic waves. Emergent arrivals and body wave velocities in excess of 1200 m/s would contribute to seismic source locations with uncertainties of several hundreds of meters.

We are able to accurately pinpoint the explosion origin time and investigate the coincidence of a seismo–acoustic source with the linear array of seven seismo–acoustic stations that were deployed at Karymksy in 1998 (Fig. 12). For a suite of 30 explosions that were recorded across this array, the apparent acoustic velocities vary from 339 to 353 m/s. These velocities could correspond to incidence angles that vary between 0 and 10° or alternatively, to temperature fluctuations ranging from 12 to 36° Celsius. Because this scatter in temperature is unrealistically large during our

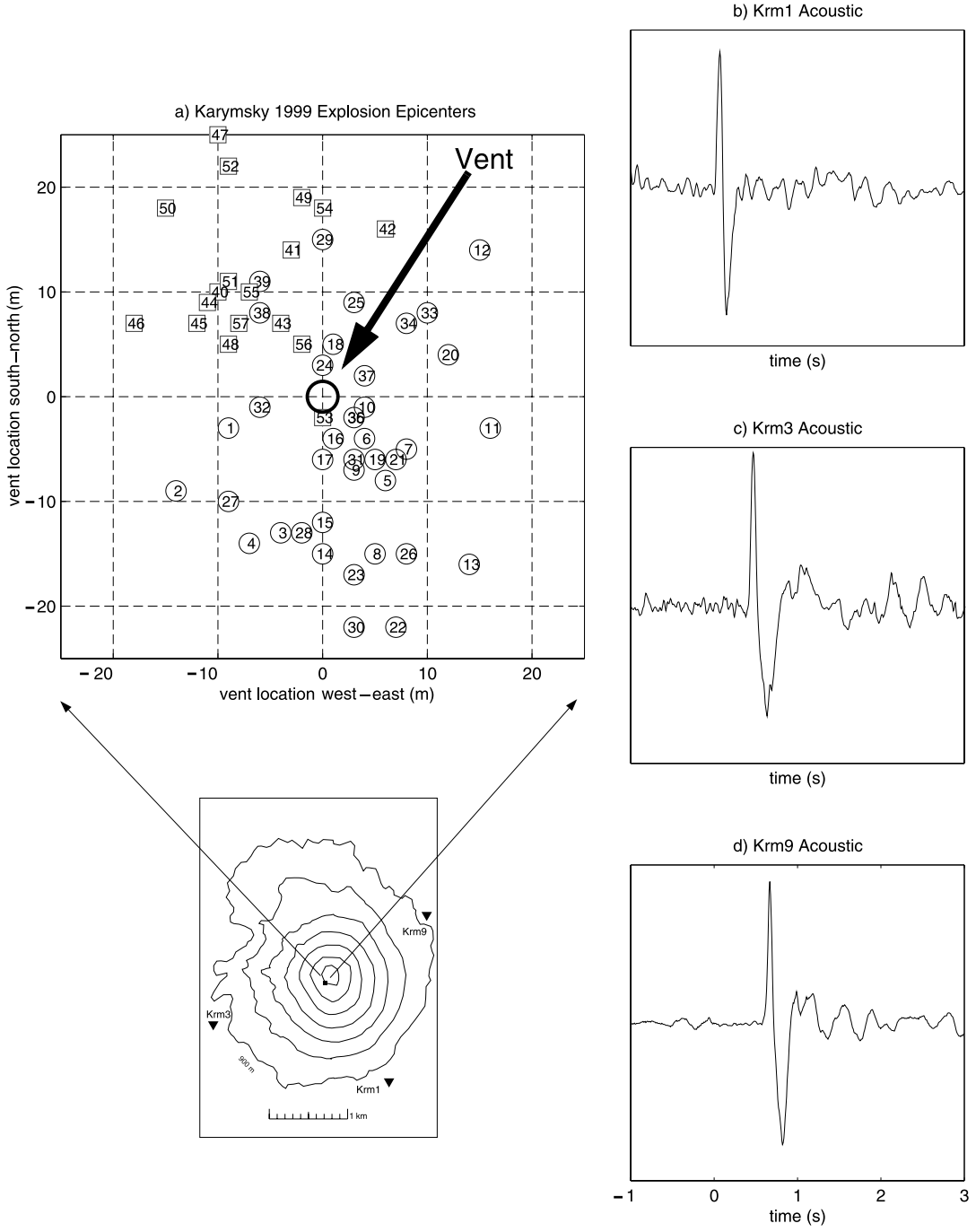


Fig. 13. Karymsky vent locations. (a) Calculated source locations determined by grid search for a suite of 57 explosions recorded between 1999:252:12:24 and 1999:255:19:25. Explosions are numbered chronologically and boxed events (40–57) are clustered temporally after 1999:254:19:59. Their spatial clustering indicates a prevailing wind out of the northwest. (b–d) Normalized pressure traces for event No. 55 (1999:255:18:09) are shown for three azimuthally distributed infrasound stations.

field campaigns at Karymsky, we infer that the incidence angle of acoustic raypaths changes according to variable atmospheric structure. A wind originating out of the northwest and blowing from the summit towards the microphone array bends acoustic energy downward so that the apparent acoustic velocity is relatively high (Johnson, in press). Despite variations in acoustic propagation velocities, the linear array can be used to recover the origin time of an explosion to within ± 0.05 s.

The origin time of the explosion source determined through analysis of seismic records is poor because of the emergent nature of the seismic waveforms. Even though the 1998 array had tight station spacing (85 m between instruments), it is still difficult to identify coherent unfiltered seismic energy crossing the array. Apparent seismic first arrival velocities can only be deduced for low-passed signals. For coherent 1-Hz energy, this apparent velocity is about 1200 ± 200 m/s. Fig. 12b displays inferred seismic and acoustic arrivals based upon a hypothetical synchronous seismo–acoustic source, using a 1200-m/s seismic velocity and a 346-m/s acoustic velocity. Although Karymsky does not exhibit precursory VLP signals like those observed at Erebus, Fig. 12b reveals that there is some emergent, short-period energy which precedes a concurrent seismo–acoustic source. The precursory seismic energy (more than 1 s in duration in some cases) is of low amplitude and could be explained either by a concurrent seismo–acoustic explosion source located at depth within the conduit, or by seismicity associated with rock failure or fluid movement prior to the explosion (Johnson and Lees, 2000). We prefer the model of precursory seismicity associated with the opening of a conduit prior to surficial gas release because it is reasonable for an explosion source that originates beneath a plug of hardened magma and rubble. Later we discuss how Pichincha Volcano possesses significant high-frequency seismicity which precedes the explosive gas release by 10 s or more.

Although some Karymsky explosions may be characterized as a single impulse (similar to Erebus infrasound), many explosions have codas which last several minutes and are indicative of extended degassing. These longer-duration events have attributes which are similar in many ways to explosions recorded at Arenal (Hagerty et al., 2000) and Sangay (Johnson and Lees, 2000). Karymsky explosion events can be grouped into several broad categories which include simple impulse events, high-frequency events, and chugging events (Johnson et al., 1998). Simple impulse events (Fig. 14a) are manifested by a single, impulsive, short-duration, damped acoustic oscillation (2–5 s long) and an associated brief seismic waveform (less than 20 s long). These seismic signals are the shortest signals associated with explosive gas release and are thus assumed to be the Green's Function response to an impulsive thrust force near the volcanic vent. Extended degassing events consist of high-frequency signals (Fig. 14b), harmonic tremor 'chugging' signals (Fig. 14c), or hybrid combinations. The high-frequency (or broad-band) events represent jetting of gases from the conduit into the atmosphere, whereas the chugging events indicate a regular sequence of gas bursts (Johnson and Lees, 2000).

Extended duration degassing events, including hybrid and chugging signals, are most common in the datasets collected in 1997 and 1999 and may reflect conduit conditions where the free flow of gas is impeded (Johnson and Lees, 2000). During the 1998 summer field season, when explosion frequency was elevated and the block lava flow was most active, virtually all events could be categorized as simple impulses. We hypothesize that a more vigorous sequence of explosions is continuously able to ream clear the conduit, enabling the near-surface system to entirely degas during a single impulsive burst. Visual observations from aerial overflights in 1997, 1998, and 1999 are consistent with the idea of a sporadically 'plugged' vent because rubble can clearly be observed choking the summit crater. Because the blocky andesitic lava at the surface is exsolved of volatiles, it may be viscous enough to prevent the upward percolation of gas (Sparks, 1997). We argue that the Karymsky explosive volatile flux must be balanced with a corresponding flux of erupted, degassed magma (Johnson and Lees, 2000).

Of the three datasets collected at Karymsky Volcano, the seismic explosion onsets from 1997

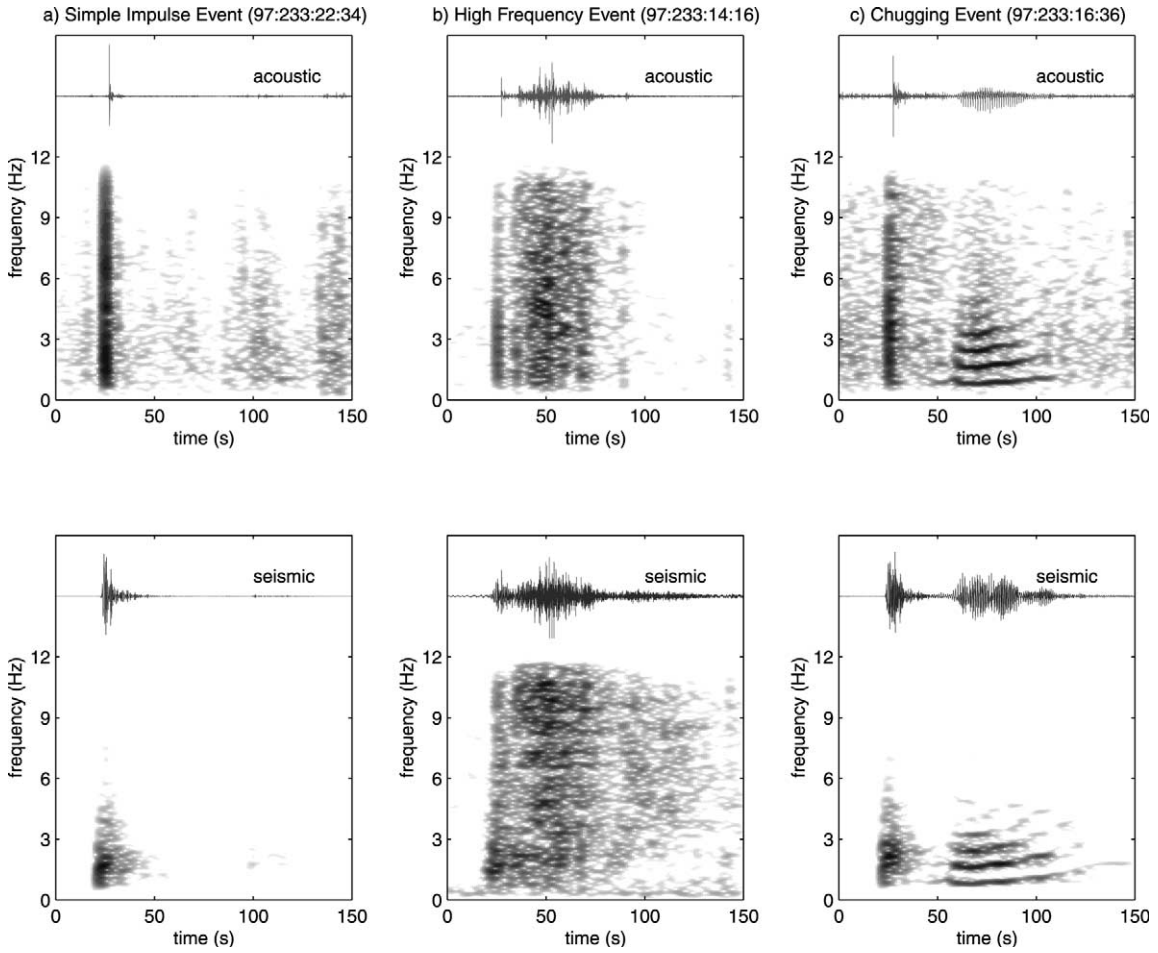


Fig. 14. Karymsky explosion types. Acoustic pressure and seismic velocity traces plotted with spectrograms for typical types of Karymsky explosions: (a) simple impulse event, (b) high-frequency event, and (c) 'chugging' event. Spectrograms are calculated with 10-s moving windows at 2-s increments and are bandpassed between 0.25 to 12.5 Hz.

are the most self-similar (Fig. 11A). Despite highly variable seismic codas (ranging from non-existent to several minutes of chugging), the first 10 s of all seismic signals have a very high degree of correlation. In 1998 and 1999, however, the onsets of seismic explosion waveforms are not nearly as repetitive. Vertical source location variability on the order of tens of meters may be sufficient to account for the lack of seismic self-similarity. Unfortunately, this amount of spatial variability is beyond the 20-m depth resolution afforded by our seismo–acoustic arrays. Experiments with closely-spaced seismic stations, such as the 1998 linear array (station spacing 85 m), demonstrate that recorded seismic signals have extremely poor semblance at neighboring stations. By reciprocity, it could take far less than an 85-m source uncertainty to account for the variability of the recorded seismic onsets in 1998 and 1999.

The deployment of well-calibrated microphones in 1998 and 1999 allowed us to evaluate and interpret the seismo–acoustic energy partitioning at Karymsky. Unlike Erebus explosion events, which

display a relatively fixed relationship between seismic reduced displacement and acoustic reduced pressure, the intensity of Karymsky infrasound appears to have little correlation with seismic amplitude (Fig. 15). For a given acoustic reduced pressure, some explosions may be seismically energetic while others are relatively weak (see double-pulsed example in Fig. 16). We attribute the variability in energy partitioning to changeable source locations within the conduit and/or muffling of the infrasonic pulse due to an overlying plug of material (Johnson, 2000). The degassed andesite choking the upper portion of the Karymsky conduit possesses a considerably higher viscosity than the Erebus phonolitic lava lake. We believe that the heightened acoustic efficiency at Erebus compared to Karymsky (Fig. 15) results from explosions which occur directly at the magma lake/free surface interface.

### 3.3. Utility of acoustic monitoring

A significant benefit of acoustic monitoring at Karymsky is the observation that complicated seismic signals, such as harmonic tremor 'chugging' events, are reflected in the infrasonic wavefield. Prior to acoustic monitoring at volcanoes such as Karymsky, seismic waveforms appeared too afflicted by complicated ground propagation filters to satisfactorily recover source locations

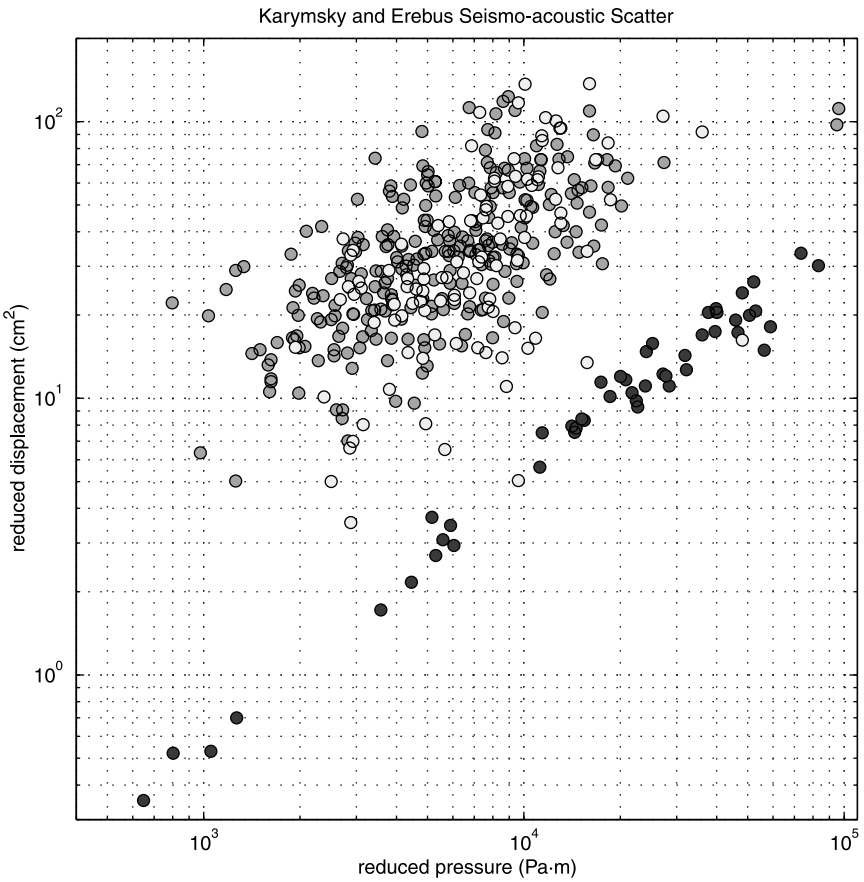


Fig. 15. Karymsky and Erebus seismo–acoustic scatter. Log–log comparison of acoustic reduced pressures and seismic reduced displacements for 427 Karymsky 1998 explosions (grey), 189 Karymsky 1999 explosions (white), and 64 Erebus 1999–2000 explosions (black).

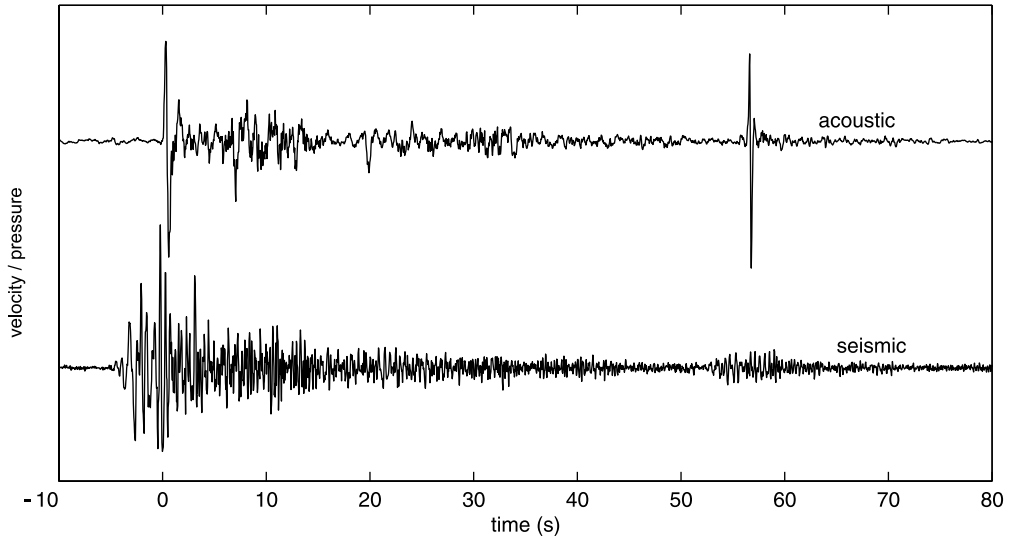


Fig. 16. Karymsky double pulse explosion with variable acoustic efficiency. Double-pulsed explosion from Karymsky (1998:248:17:02) demonstrates a rapid change from low acoustic efficiency (relative to seismic) to high acoustic efficiency for the second pulse.

or mechanisms. Infrasonic data from Karymsky demonstrate that the dramatic and rapid expansion of compressed gas at the free surface is the most likely mechanism for the seismic source (including complicated, extended-duration seismo–acoustic codas). The recorded seismic waveforms are thus a heavily filtered, heavily scattered response to a gas expansion thrust force at the vent. Some limited low-amplitude precursory seismicity, which is not reflected in the infrasonic channel, may reflect processes that are not associated with gas release.

Our seismo–acoustic experiments at Karymsky also provide greater insight regarding the conditions inside a volcanic conduit during an eruption. Acoustic efficiency (relative to seismic) may be an important indicator of either the depth of an explosion source or the physical properties of the conduit and fluid. Variations in the type of explosion may reveal the ease with which gas is able to escape to the free surface. At Karymsky, we observe that successive explosions, whether they are simple impulse, high-frequency, or harmonic tremor events, tend to be of the same variety (Fig. 17). These varied explosion types may result from factors such as conduit dimensions, fragmentation depth, and/or plug characteristics (Johnson and Lees, 2000). Event clustering suggests that these conduit and plug parameters evolve gradually over the course of several explosions.

## 4. Sangay (1998)

### 4.1. Background

Sangay Volcano (Fig. 18) is located in Ecuador's eastern cordillera at the southern terminus of the Northern Andes volcanic zone. It is the most continuously active volcano in Ecuador with recorded activity extending back to at least 1628 (Hall, 1977). Typical Sangay behavior ranges from vigorous explosions with mass ejecta, dome growth, and pyroclastic flows, to less violent explosions with a predominance of gas release. Due to its isolated position in the cloud-shrouded eastern cordillera of Ecuador, fluctuations in the type of activity frequently occur without notice. Sangay is a 5230-m stratovolcano with an edifice height of more than 1800 m and a complex summit of four aligned craters distributed along a 700-m ridge (Monzier et al., 1999). During the April 1998 field season, eruptive activity was at a relative low level, with discrete Strombolian-

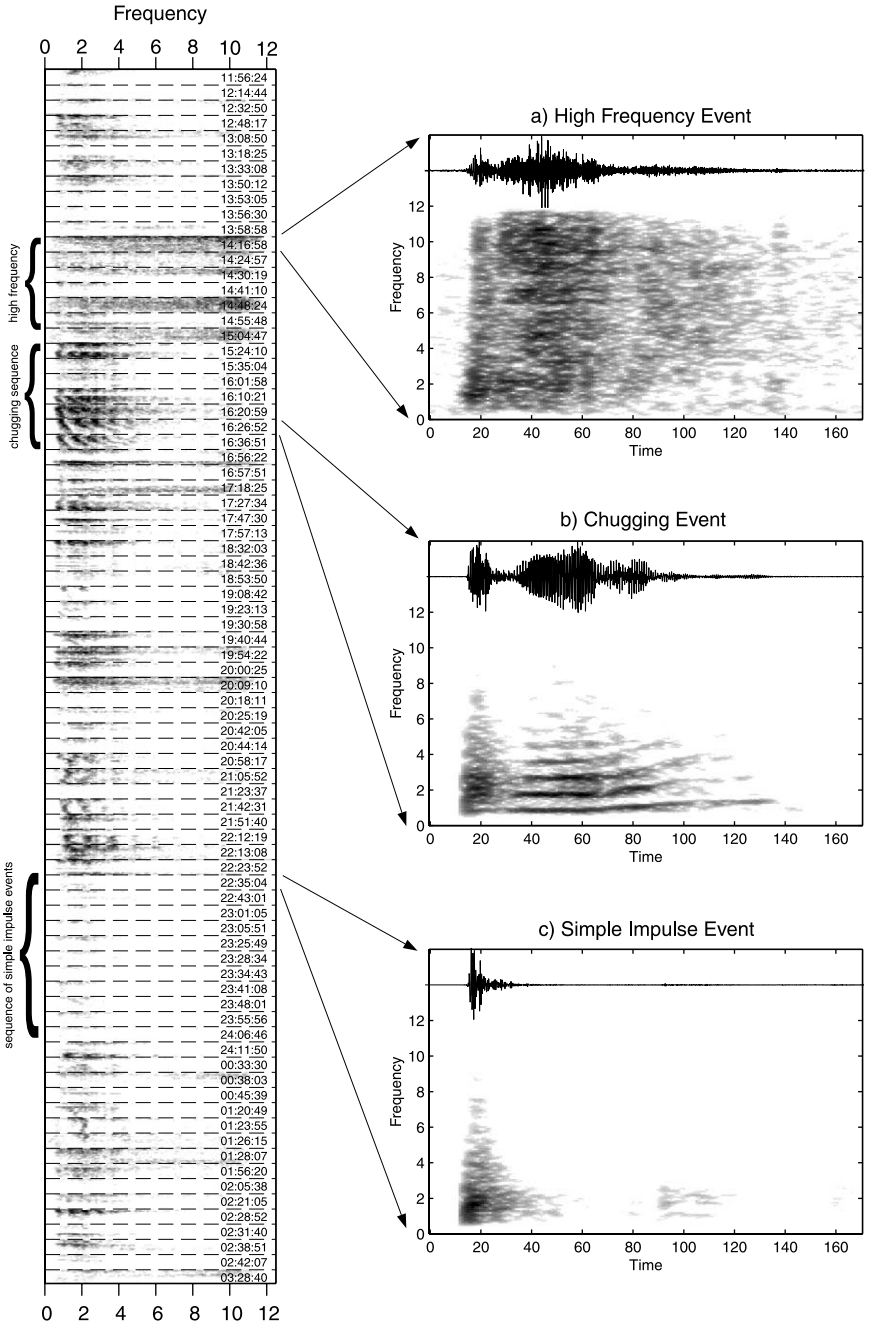


Fig. 17. Karymsky event evolution. Seismic traces and associated spectrograms for three characteristic event types at Karymksy in 1997: (a) high-frequency event, (b) chugging (harmonic tremor) event, (c) simple impulse event. The spectral evolution plot demonstrates how specific event types tend to cluster in time for the Karymsky 1997 record. Spectrograms are calculated for 80 consecutive events using time windows 30–90 s after the explosion onset. Figure is reproduced from Johnson and Lees (2000).

Fig. 18. Sangay Volcano. Windblown plume from Sangay in 1996. Photo courtesy of P. Hall.

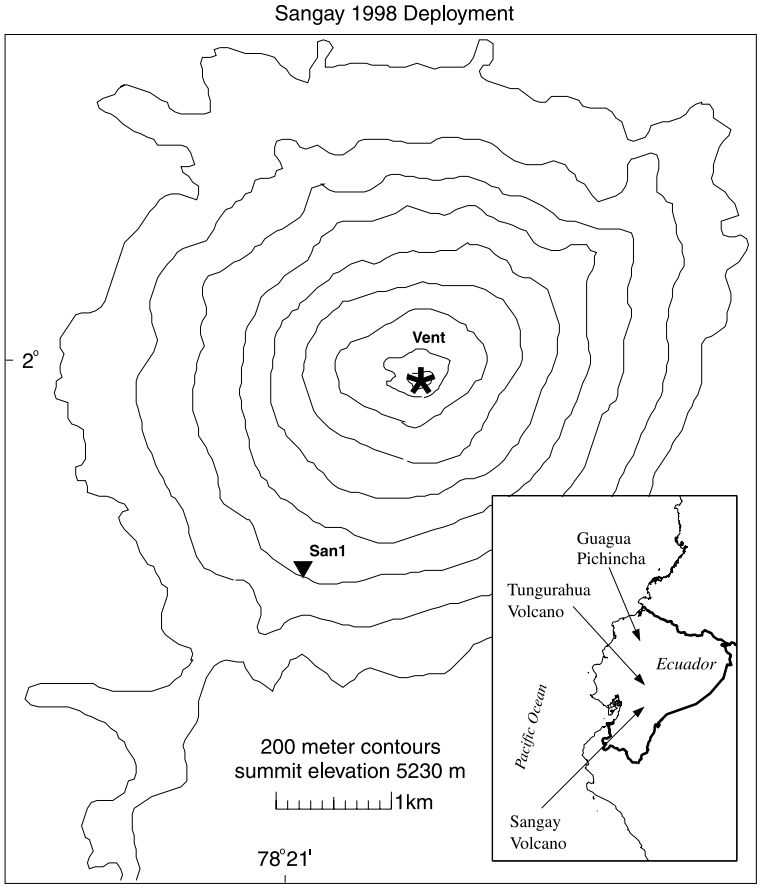


Fig. 19. Map of Sangay station; Sangay 1998 deployment. Station San1, located 2200 m from the active vent, contained both a seismometer and microphone.

type explosions emanating from a single vent approximately twice each hour. Some ejecta and the observation of incandescence hinted at a slight, but continuous flux of solid material through the vent. Though Sangay's chemical composition is variable, the bulk of recent lavas is basaltic andesite or andesite (Monzier et al., 1999). Based upon silica content, the viscosity of the erupting magma may be comparable to the magma emerging from Karymsky between 1997 to 1999 (Sparks, 1997).

We recorded Sangay explosions with acoustic and seismic instruments during a five-day period in April, 1998. During this experiment we co-located a single Venema microphone with a CMG 40-T seismometer 2200 m from the active vent at station San1 (Fig. 19). Data acquisition on a portable PASSCAL Reftek A-08 datalogger was con-

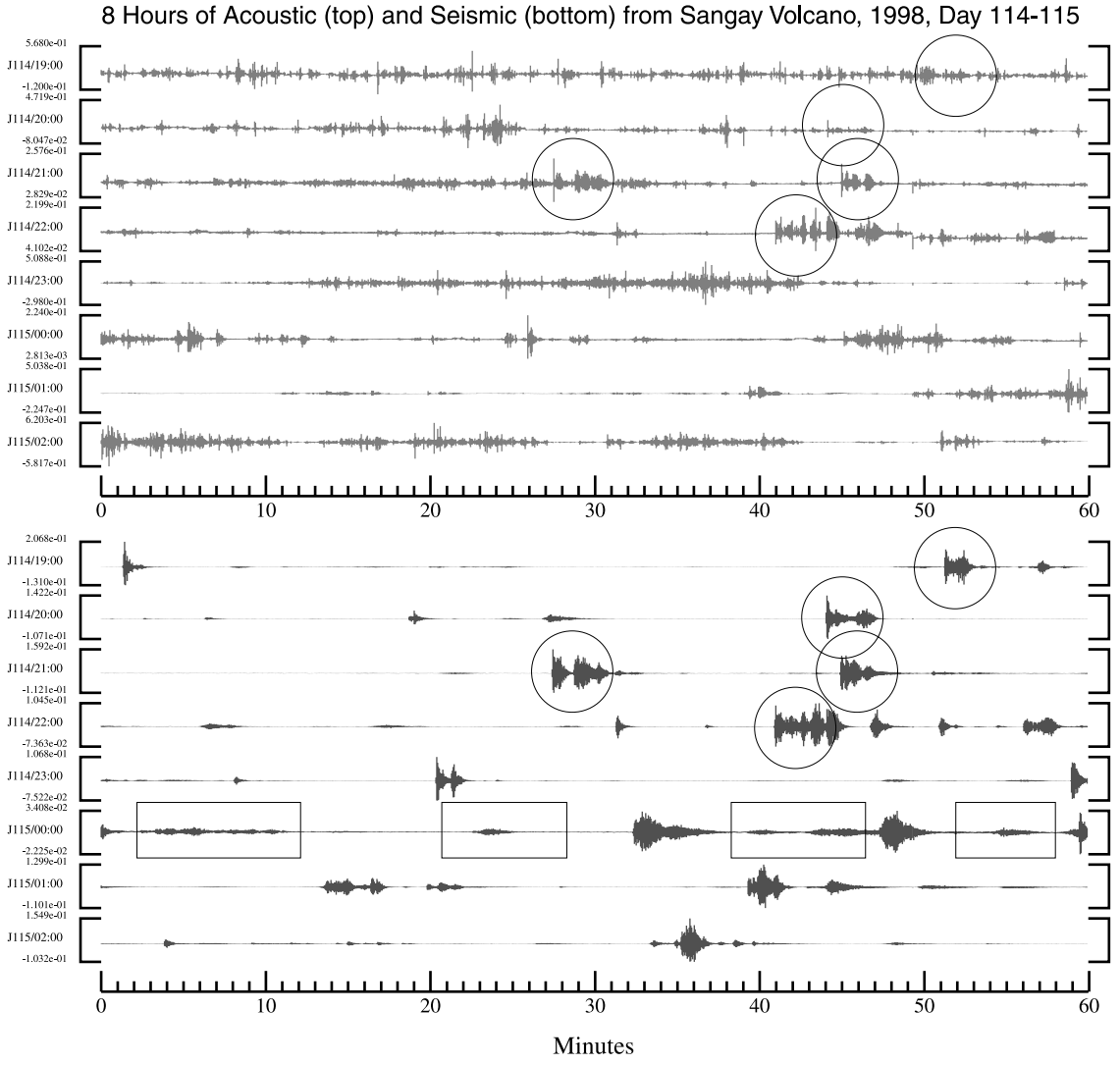


Fig. 20. Sangay 8-hour acoustogram and seismogram. Eight hours of activity recorded at station San1, day 114 and 115, 1998. Acoustic signals are recorded with a Venema microphone (top) and seismic signals are recorded with a CMG-40T broadband seismometer (bottom). Circled events correspond to the explosions displayed in Fig. 21. Boxed events are seismic tremor signals without obvious acoustic counterparts.

tinuous at 125 samples per second. Our experiment was the first to digitally record Sangay volcanic earthquakes with either seismic or acoustic sensors.

### 4.2. Data overview

Acoustic noise proved problematic during our study at Sangay because of persistent high winds

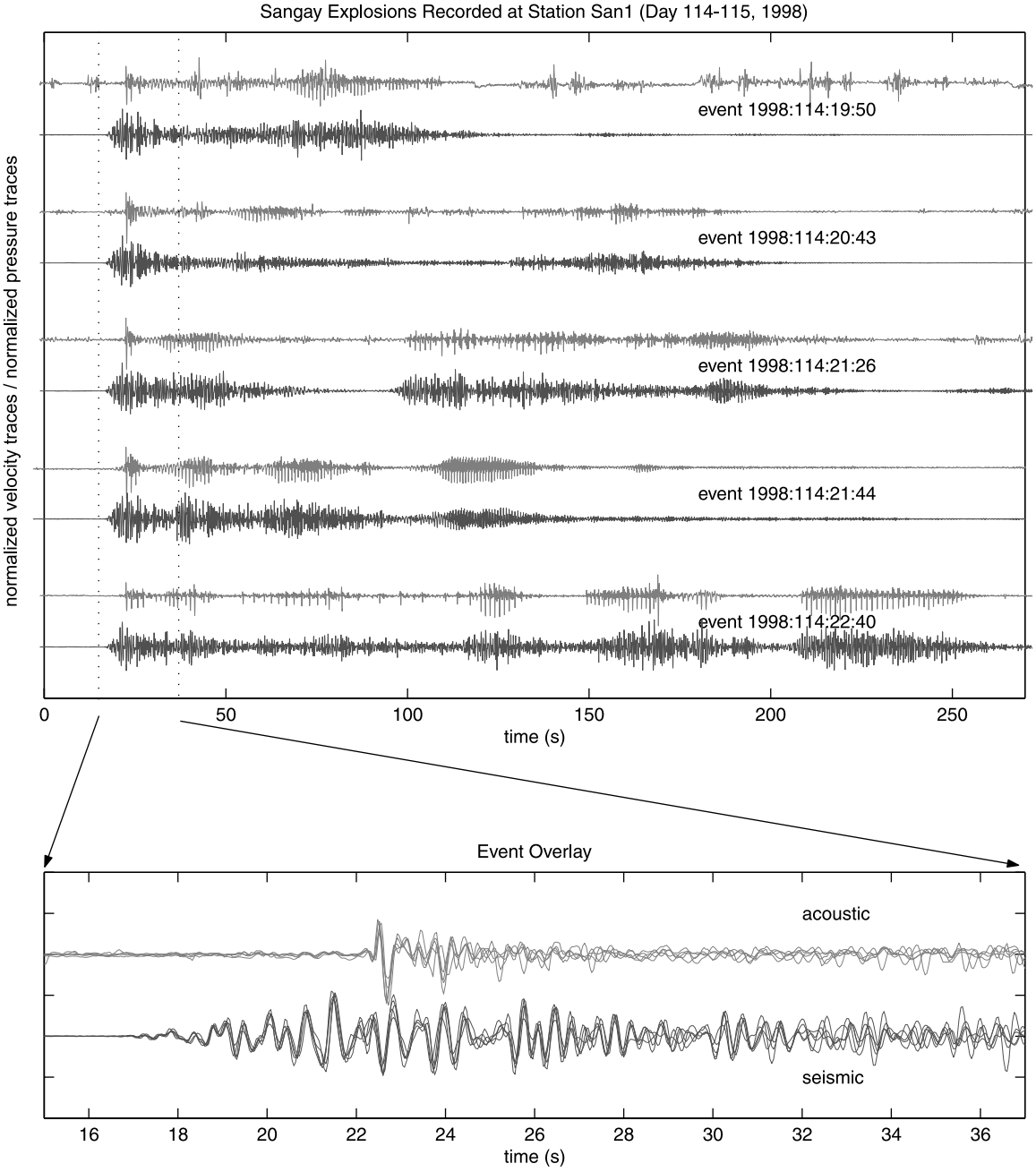


Fig. 21. Sangay explosion examples. Selected normalized explosion waveforms from Fig. 20 (indicated by circles).

at the recording site and the relative infrequence of explosions compared to Karymsky (Fig. 20). As a result, the Sangay dataset contains only about 50 events of good acoustic quality, corresponding to about 40% of all the explosions identified on the seismic channel. Unlike the recorded Karymsky seismicity, it is possible that some significant seismic signals from Sangay may not be associated with surface degassing (see tremor signals denoted by boxes in Fig. 20 for possible candidates). However, it is impossible to definitively determine whether these sources are internal owing to a relatively high background acoustic wind noise which would obscure associated infrasound.

Sangay explosions, like Karymsky and Erebus explosions, are characterized by a fixed travel time difference between seismic and acoustic phases. Applying reasonable sound speed velocities (330 m/s), a concurrent seismo–acoustic source would imply that seismic first arrivals have a velocity of $1600 \pm 300$ m/s. This velocity is approximate because of the emergent nature of the seismic signals and the assumption that seismic and acoustic onsets correspond to the same source origin time. Despite their emergent nature, the onsets of the seismic waveforms are generally self-similar (Fig. 21) indicating repeatable source locations and motions for the very beginning of explosive degas-

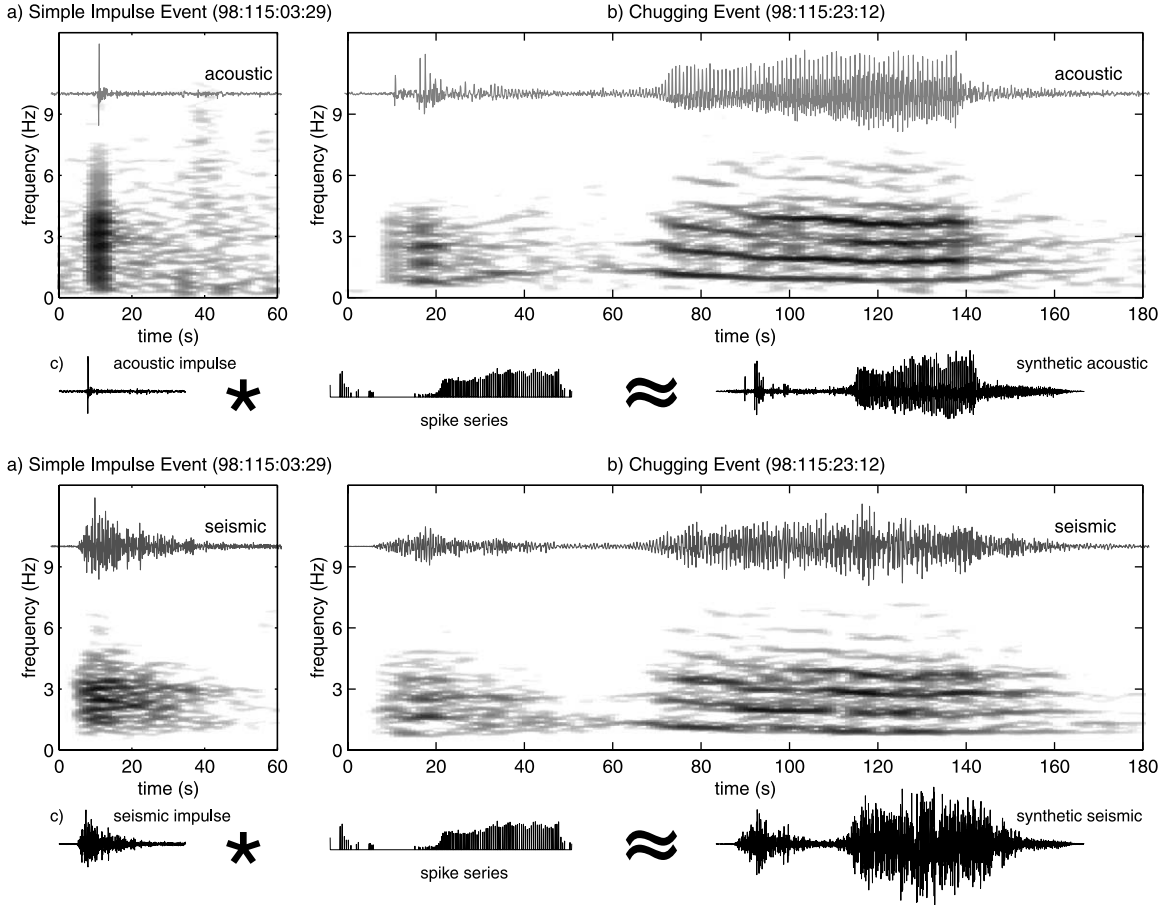


Fig. 22. Sangay simple impulse and chugging event. Example traces and spectrograms of: (a) rare Sangay simple impulse explosion, and (b) common Sangay chugging explosion. Both traces are bandpassed between 0.25 and 12.5 Hz. Associated spectrograms are calculated with a 10-s moving window at 2-s increments. The fundamental frequency of the harmonic tremor signals corresponds to the time interval between individual acoustic pulses. (c) Sangay chugging events can be thought of as a series of gas releases or a convolution of a simple impulse event with a spike series corresponding to the sequence of chugs.

sing. The onsets of all acoustic explosion signals from Sangay, like those from Karymsky, are impulsive, making it very easy to identify acoustic arrival times.

The primary difference between the Sangay and Karymsky explosions is that virtually all events recorded at Sangay possess an extended coda. In many explosions, spectacular harmonic tremor 'chugging' events last several minutes with 'gliding' of the fundamental frequency between 0.4 and 1.5 Hz (Fig. 22). These seismo–acoustic chugging events are remarkably similar in appearance to the chugging events recorded at Karymsky in 1997, hinting at a similar degassing mechanism. During the 1998 Sangay field season a relatively low magma flux and infrequent explosions suggest that a high-viscosity plug of rubble had the opportunity to form in the conduit which may have been responsible for the near omnipresence of chugging explosions (Johnson and Lees, 2000).

### 4.3. Utility of acoustic monitoring

The physical conditions responsible for the 'chugging' phenomena at Sangay and Karymsky may be replicated at a host of other volcanoes where chugging has also been documented: Arenal, Costa Rica (Benoit and McNutt, 1997), Semeru, Indonesia (Schlindwein et al., 1995), and Langila, Papua New Guinea (Mori et al., 1989). Because Karymsky and Sangay chugging is evident in both acoustic and seismic channels and is associated with visible degassing, it provides an opportunity to understand source mechanisms for this distinct type of volcanic harmonic tremor. The periodicity of the pulses, which range from 0.4 Hz at Sangay to 1.5 Hz at Karymsky, is sufficiently regular to produce integer overtones in the frequency spectra (Fig. 22). Explanations for the remarkable regularity of the explosion pulses include: resonating fluid bodies (Benoit and McNutt, 1997; Schlindwein et al., 1995; Garces and McNutt, 1997), Von Karmon vortice shedding (Hellweg, 2000), and choked flow through a pipe (Julian, 1994; Lees and Bolton, 1998). A choked-flow model appears to be a reasonable explanation for Karymsky and Sangay harmonic tremor, where gas may be escaping through cracks or narrow conduits in a viscous, blocky lava, before venting at the surface.

## 5. Tungurahua (1999)

### 5.1. Background

Tungurahua Volcano (summit elevation 5016 m) is a large stratovolcano with 3000 m of vertical

Fig. 23. Tungurahua Volcano. Eruption plume as seen from near the town of Pelileo on October 23, 1999.

relief located in Ecuador's eastern cordillera 60 km to the north of Sangay (Fig. 23). Prior to the current period of activity, Tungurahua last erupted between 1916 and 1918, producing Strombolian explosions, andesitic lava flows, and a few pyroclastic flows towards the end of the eruption (Hall et al., 1999). Heightened seismicity, first noted in September 1999, preceded the current eruption by about one month. Continuous seismic tremor steadily increased in energy until magma finally breached the surface on October 5, 1999. The initial eruption was characterized by periods of Vulcanian activity with convective plumes rising more than 5 km above the vent, significant ash fall to the west and southwest of the volcano, and small lahars. Between November 1999 and October 2000, eruptive vigor steadily decreased towards more intermittent Strombolian activity, with more energetic eruptive phases commencing again in May of 2001.

We deployed a McChesney 4-element electret condenser microphone with a short-period seismometer 9 km from the vent to assess the quantity and relative magnitude of the Tungurahua

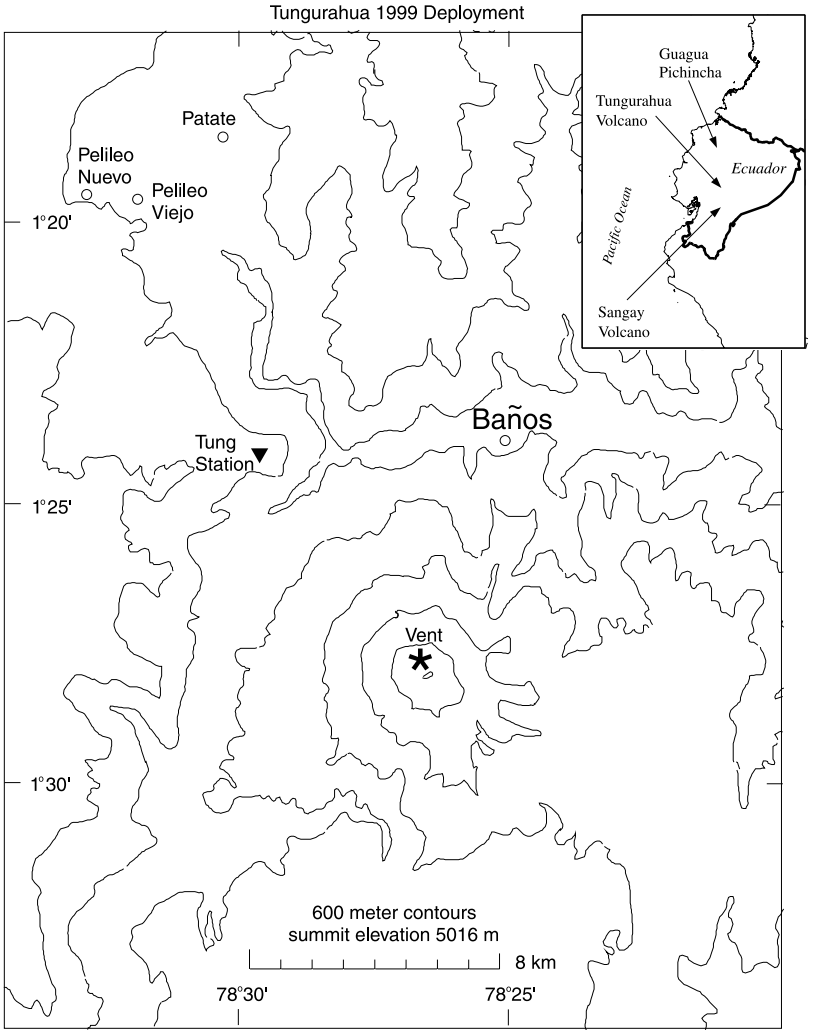


Fig. 24. Map of Tungurahua station. The temporary station Tung, deployed in October 1998, contained a short-period seismometer and a 4-element McChesney-type microphone.

explosions (Fig. 24). All seismo–acoustic data were recorded continuously at 50 samples per second on a Pacific Northwest Seismograph Network (PNSN) Reftek A-07 datalogger. The data presented here are from a 4-day period, beginning October 23, 1999, when activity was characterized by an almost continuous series of explosions, emissions of gas and ash columns several kilometers high, and the ejection of large incandescent blocks.

### 5.2. Data overview

The initial motivation for deploying a low-frequency microphone at Tungurahua was to assess remotely the eruptive vigor and frequency of the

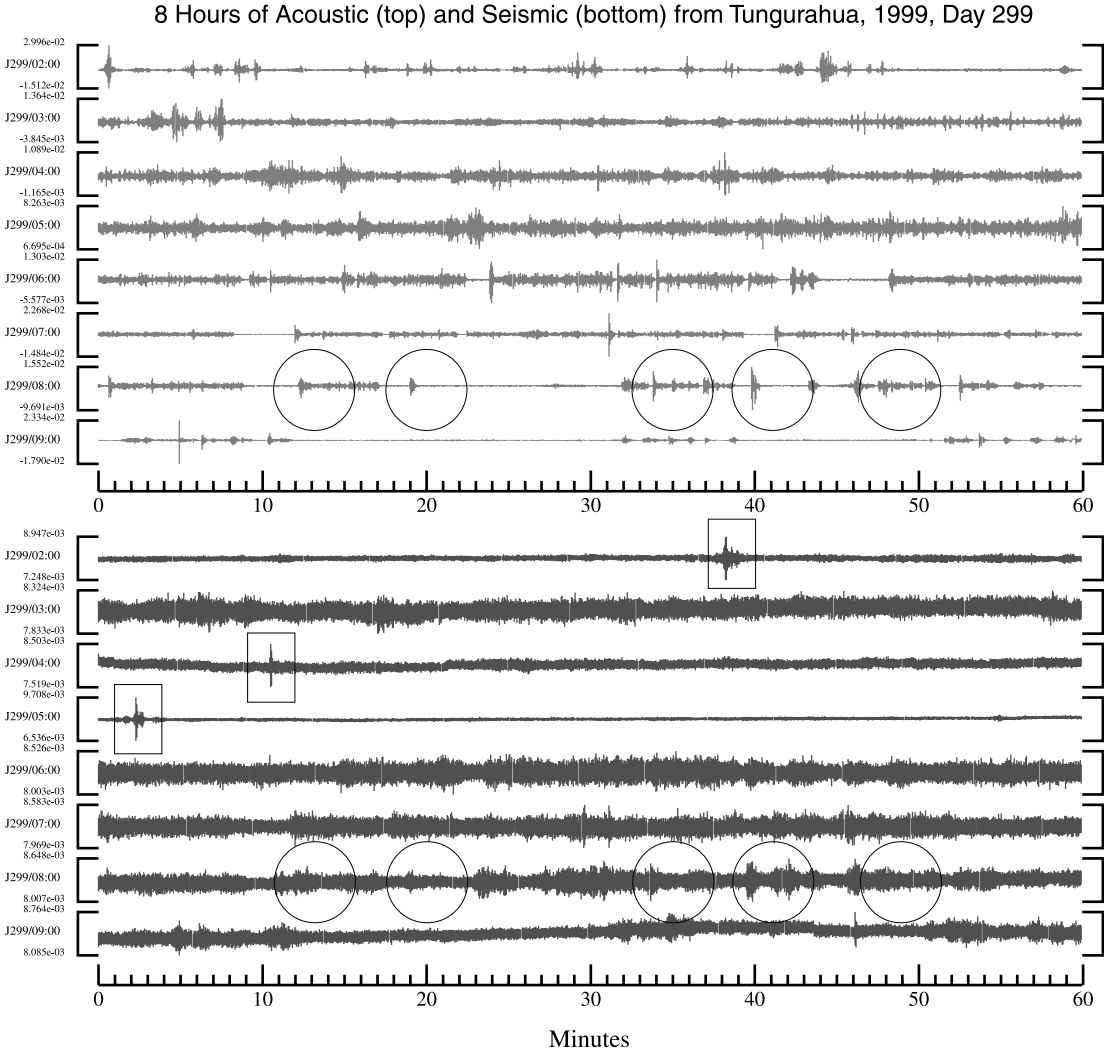


Fig. 25. Tungurahua 8-hour acoustogram and seismogram. Eight hours of activity recorded at station Tung, day 299, 1999. Acoustic signals are recorded with a 4-element McChesney-type microphone (top) and seismic signals are recorded with a Mark Products short-period seismometer (bottom). Acoustic traces have very low wind noise and are records of eruptive degassing. The high-amplitude seismic tremor is noise that is mostly unassociated with volcanic explosions. Higher amplitude discrete events (indicated by boxes) are regional earthquakes. Circled events correspond to discrete explosions that are displayed in greater resolution in Fig. 26.

volcanic explosions. Acoustic monitoring proved particularly beneficial at Tungurahua because seismic channels were plagued by very energetic volcanic tremor even prior to the commencement of the 1999 eruption. Pre-eruptive seismic tremor is thought to be related to hydrothermal fluid movement at Tungurahua because increased seasonal tremor amplitude has been positively correlated with periods of heavy rain (Ruiz et al., 1999). In the weeks preceding and during the eruptions of October 1999, tremor amplitude increased and became intense enough to saturate short-period stations 5 km from the vent. Through the end of October this tremor effectively obscured seismic signals associated with explosion earthquakes (Fig. 25). Since discrete explosions were identifiable both audibly and visually, we deployed our low-frequency acoustic microphone as a supplementary monitoring tool. Despite its 9-km distance from the vent, the microphone allowed us to successfully identify a suite of different infrasonic signals during periods of low wind (late afternoon to mid-morning).

During periods of low wind, impulsive acoustic bursts and longer-duration acoustic tremor (Fig. 25) occur almost continuously and correspond to visual observations of gas and ballistic emissions. Relative quiet precedes impulsive infrasonic sig-

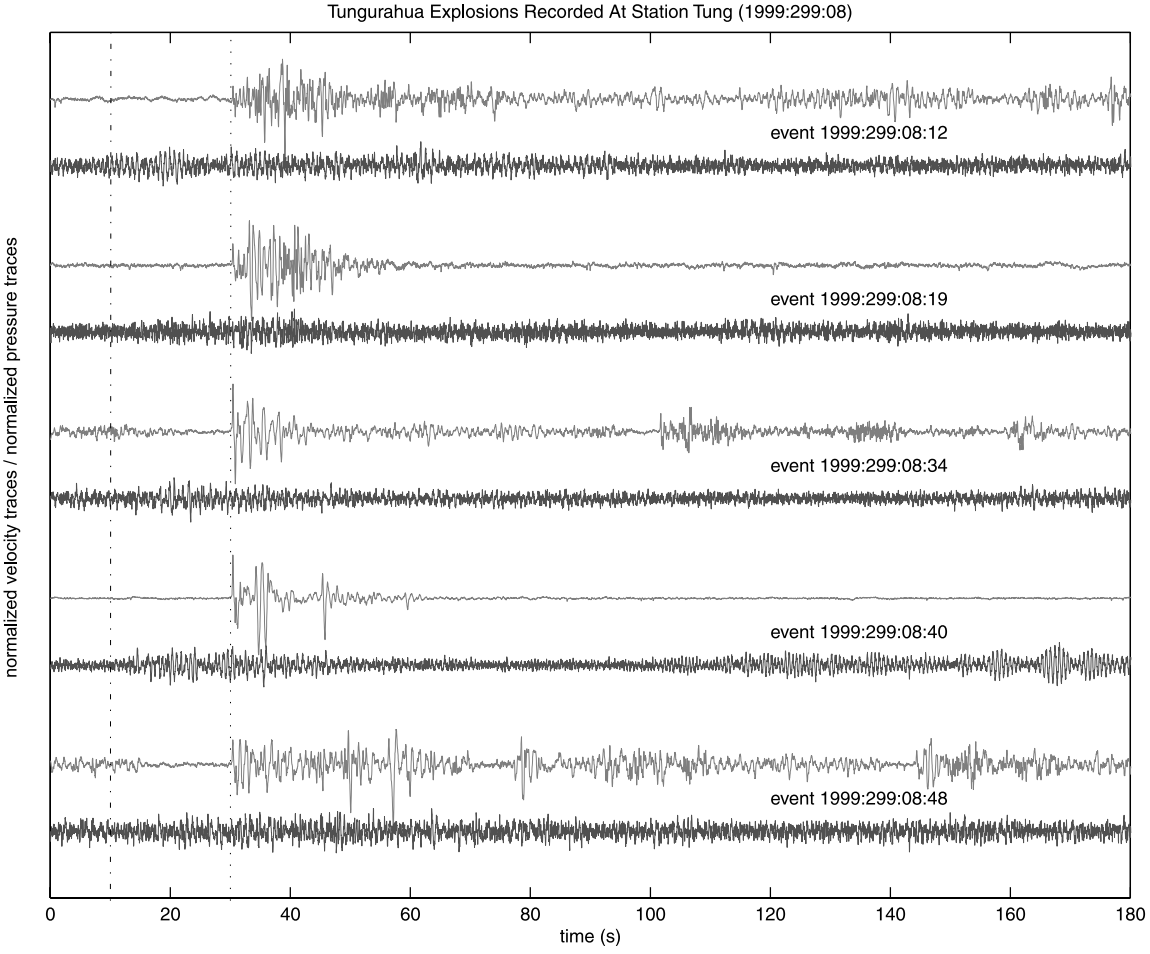


Fig. 26. Tungurahua explosion examples. Selected normalized acoustic (top trace) and seismic (bottom trace) waveforms from Fig. 25 (indicated by circles).

nals in only a few instances (Fig. 26). Tungurahua's explosive activity thus differs significantly from the discrete Strombolian-type explosions that characterized activity at Erebus, Karymsky, and Sangay Volcanoes. In general, the Tungurahua infrasound is poorly correlated with seismicity because of ubiquitous, noisy seismic background tremor. In theory, the seismic arrivals at station Tung should precede the acoustic arrivals by approximately 25 s for a common seismo–acoustic explosion source (applying reasonable seismic and acoustic propagation velocities). However, associated packets of seismic and acoustic energy are only barely evident in the spectrograms of Fig. 27. Only towards the end of the October 2000 eruptive phase, was background seismic noise sufficiently diminished to allow easy correlation between seismic and infrasonic explosion signals (Ruiz et al., 2001).

Because of the relatively lengthy propagation distances between the vent and the seismo–acoustic station Tung (~9 km), higher frequency infrasound is attenuated and the bulk of the recorded acoustic energy appears to lie below 5 Hz (Fig.

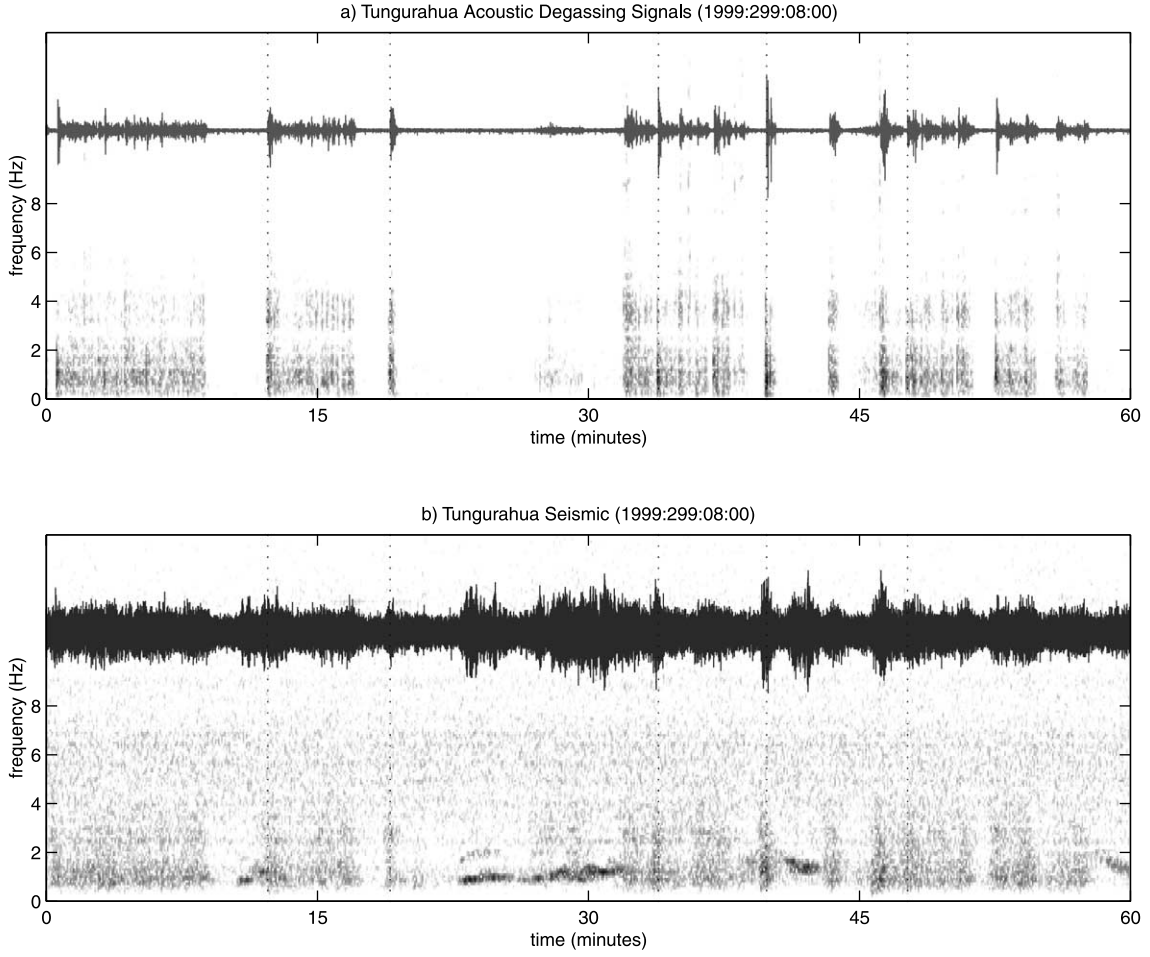


Fig. 27. Tungurahua spectrogram. Seismic and acoustic traces with associated spectrograms for 1 h of degassing activity at Tungurahua Volcano. (a) The acoustic trace shows a combination of impulses and continuous tremor with a characteristically double-peaked frequency spectrum. (b) The seismogram has only a slight correlation with the acoustogram (most evident in the accompanying spectrograms).

27). An additional unexplained absence in acoustic energy at about 3 Hz, which is not observed in infrasonic signals from other volcanoes, may be a unique property of the Tungurahua eruption source. This double-peaked acoustic frequency spectrum provides an effective diagnostic tool for distinguishing between degassing signals and wind noise. Though wind noise is often severe enough to completely mask Tungurahua eruption signals, the wind spectrum is broad-band and contrasts dramatically with the double-peaked degassing spectrum.

### 5.3. Utility of acoustic monitoring

During periods of low wind, the microphone deployed at Tungurahua served as an effective tool for determining when an eruption was in progress and the general nature of degassing. Frequent inclement weather, a large inaccessible zone around the volcano, and noisy seismic data made verification of gas and material flux from the vent difficult to monitor without independent infrasonic observations. The infrasound signals recorded at Tungurahua indicate a continuous style of degassing, consisting of both explosive pulses and quasi-continuous 'jetting'. The associated eruptive activity during October 1999 is also somewhat more vigorous than the Strombolian activity recorded at Erebus, Karymsky, or Sangay. Though Tungurahua magma viscosity may be similar to Karymsky and Sangay, enhanced gas and magma flux at Tungurahua probably account for the heightened eruptive vigor.

As a quantitative tool, the microphone deployed at Tungurahua had several shortcomings. The distant location of the station made absolute pressure measurements inexact due to the vagaries of acoustic transmission through 9 km of atmosphere. At such distances, relative acoustic amplitudes are likely to be extremely dependent upon variations in the atmospheric temperature and wind structure, which changes throughout the day. Finally, a lack of clean seismic records and visual observations hinders the analysis of Tungurahua infrasound. A future seismo–acoustic study at Tungurahua would benefit from better visual observations, multiple microphones, and closer proximity of seismo–acoustic stations to the vent.

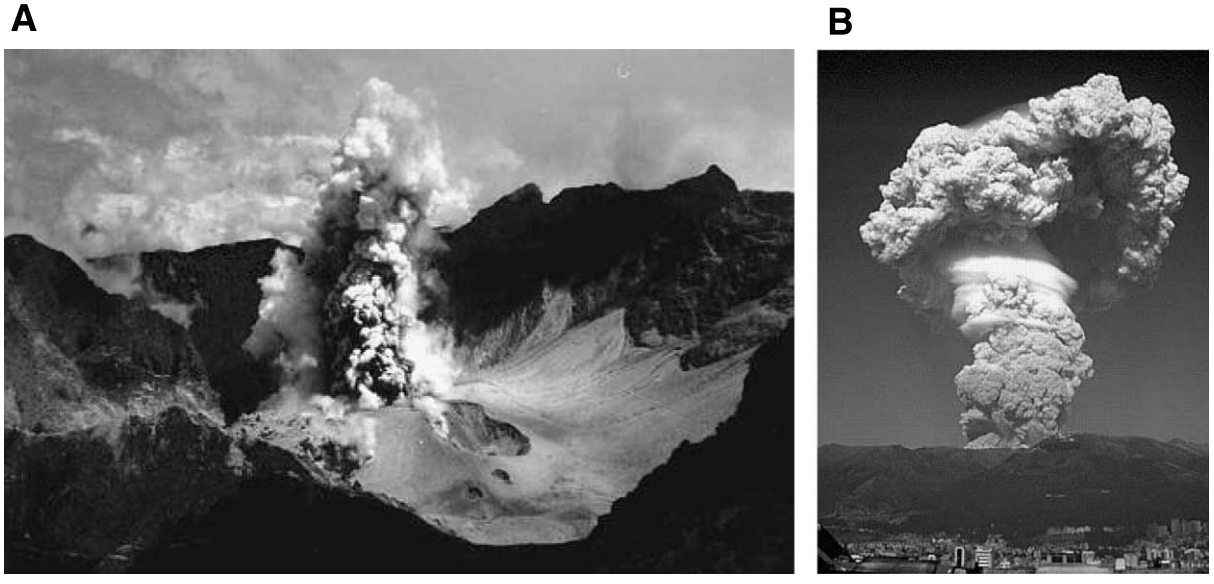


Fig. 28. Pichincha Volcano. (a) August 2, 1999, explosions from dome as seen from near the summit of Pichincha. Photo courtesy of F. Rivadeneira. (b) View from Quito of October 7th, 1999, convective plume rise associated with a possible partial dome collapse. Photo courtesy of M. Quito.

## 6. Guagua Pichincha (1998–1999)

### 6.1. Background

Guagua Pichincha (summit elevation 4739 m) is a stratovolcano with a horseshoe-shaped caldera 1.5 km wide that partially encloses an active dacite dome (Fig. 28A). The previous significant eruption of Pichincha occurred in 1660 and was associated with the deposit of several centimeters of ash in Quito, 12 km to the east (Hall, 1977). In recent decades, until the onset of the volcanic crisis in 1998, activity at Pichincha was characterized by vigorous fumaroles on the dome and infrequent phreatic explosions (several each year). The summer of 1998 marked a dramatic increase in phreatic explosions (several each week), culminating in swarms of volcano–tectonic (A-type) earthquakes in mid-September 1999. The first magmatic eruption occurred on September 26th, dropping some ash on southern Quito. New dome growth was first noted at the end of the month. On October 7th, 1999, dome destruction was associated with a spectacular convective plume rising 5 km that was clearly visible from Quito (Fig. 28B). This event was responsible for the demise of

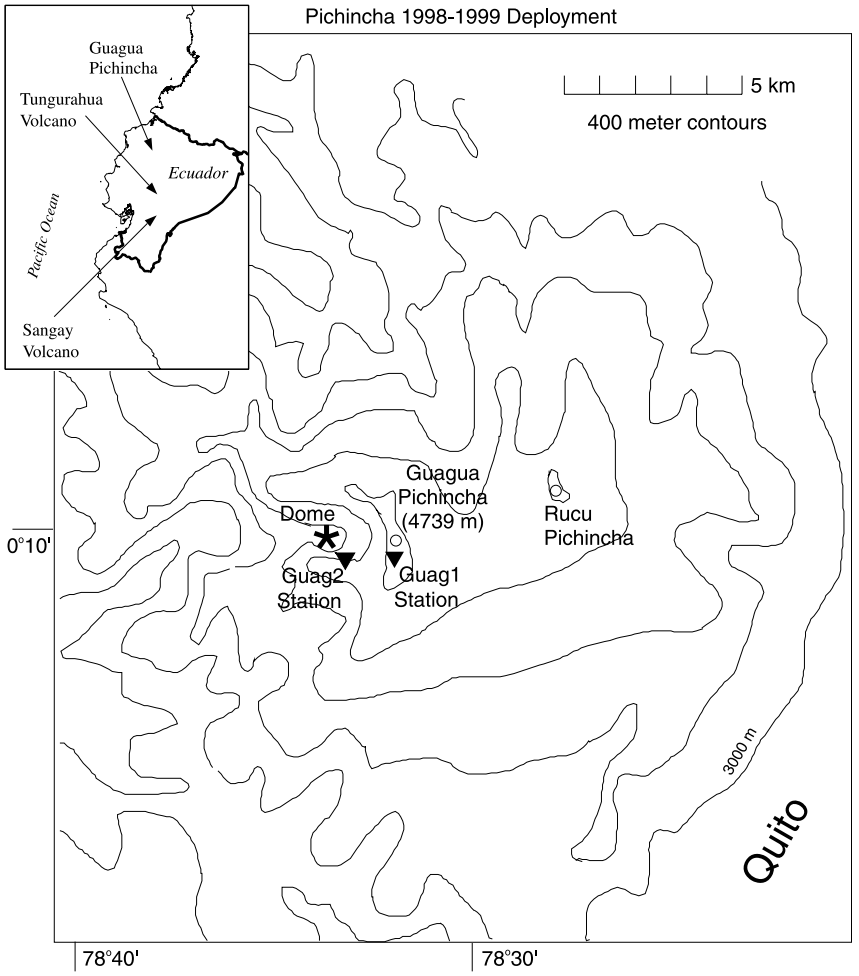


Fig. 29. Pichincha 1998–1999 low-frequency station locations. Network seismic station CGG is situated at Guag1. The microphone at Guag1 was a single-element Venema microphone that was operational until June, 1999. Station Guag2 contained a McChesney 16-element microphone array which operated from June 1999 until October 1999.

our microphone at Guag2, located 600 m from the vent. Repeated episodes of dome growth and subsequent dome destructions continued throughout 1999.

We established a telemetered acoustic microphone in November 1998 in order to monitor phreatic activity in Pichincha. This microphone and its replacement operated almost continuously until October 1999. The first installation employed a single electret condenser Venema microphone, co-located with a short-period single-component network seismometer, 1500 m from the vent at station Guag1 (Fig. 29). In June, 1999, we upgraded the single-element condenser microphone to a McChesney 16-element, 4-m aperture, electret condenser microphone array. This replacement microphone was co-located with a network seismometer stationed 600 m from the vent at Guag2. Both microphones were deployed primarily to help differentiating between explosion events and shallow sub-surface seismicity. Acoustic and short-period seismic data were telemetered to the Instituto Geofisico of the Escuela Politecnica Nacional in Quito for real-time evaluation.

### 6.2. Data overview

We replaced the single-element microphone at Guag1 with the 16-element microphone array at Guag2 because it appeared as though acoustic signals at Guag1 were obscured by high levels of wind noise. Indeed, wind was consistently strong at station Guag1, which was located near the summit of Pichincha. Out of approximately 100 possible phreatic explosions (identified through analysis of the seismic records), only about a dozen events have clear associated infrasonic pulses similar to those exhibited at other volcanoes. Interpretation of the seismo–acoustic signals recorded at Guag1 is hampered by a lack of first-hand audio or visual observations of the eruptive activity. It is therefore not entirely apparent which seismograms correspond to explosive gas release.

One of the most interesting observations from

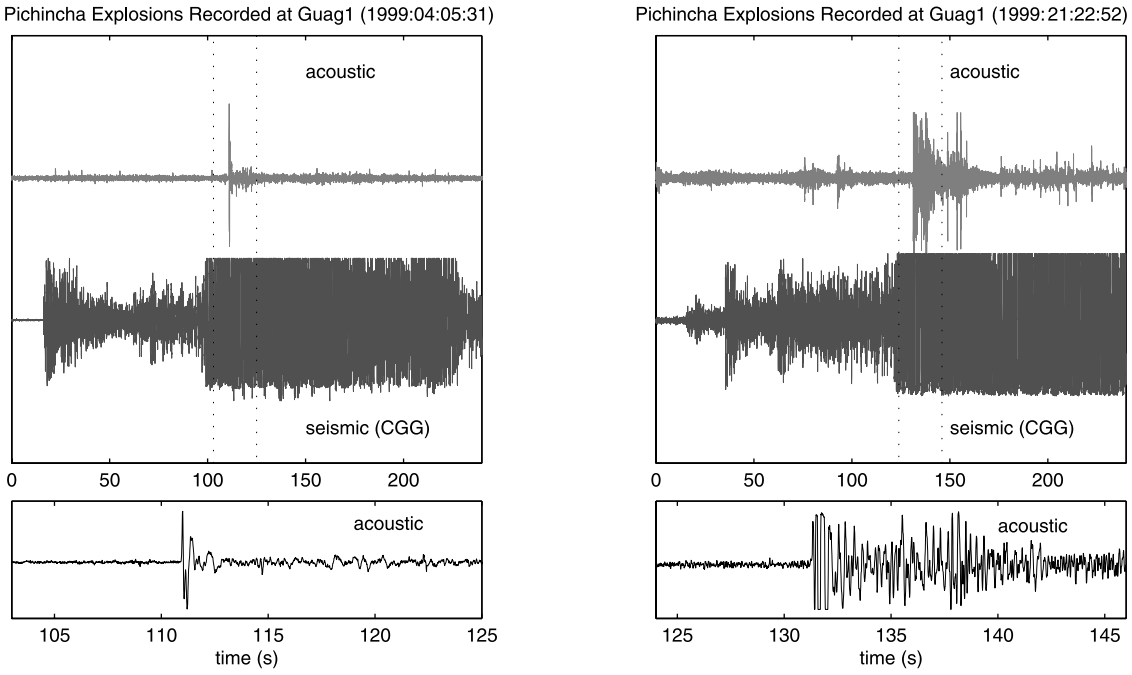


Fig. 30. Pichincha explosion examples from Guag1. Two normalized explosion waveforms recorded acoustically at station Guag1 (top trace) and seismically at station CGG (bottom trace). Signals are clipped due to dynamic range limitations of the telemetry. Enlargements of a portion of the acoustic pressure traces are included in separate panels.

the Guag1 data, is that acoustic pulses do not follow the onset of seismic signals by a fixed, predictable time interval. At an epicentral distance of 1500 m, travel time difference between the seismic and acoustic phases should be approximately 4 s for a concurrent seismo–acoustic vent source. However, the phreatic explosions recorded at Guag1 show acoustic arrivals lagging seismic arrivals by 60 s or more (Fig. 30). This delay indicates that either sub-surface seismicity precedes gas release from the vent or that the initial venting of gas is too insignificant to register on the acoustic channel.

We designed and implemented the 16-element microphone at Guag2 to improve the acoustic signal-to-noise ratio. Closer proximity to the vent, deployment in the lee of a ridge, and the spatial filtering of 16 individual sensors resulted in generally low wind noise. However despite wind noise reduction, clear impulsive acoustic signals were not forthcoming. Obvious acoustic degassing signals are associated with only a minority of the possible explosion events identified from seismic records (Fig. 31). When infrasonic explosion signals are present, they tend to be relatively broad-band (1–15 Hz), tremor-like, emergent, and follow the seismic onsets by as much as 90 s. Based upon interpretation of seismic and infrasonic records, the explosion sources at Pichincha during the summer of 1999 are dramatically different from those at Erebus, Karymsky, Sangay, and Tungurahua. Only a few eyewitness reports are available, but they appear to confirm an entirely different degassing mechanism. These reports describe continuous 'jetting' noises and longer-duration degassing instead of the 'booming', 'chugging', or 'puffing' associated with Strombolian activity.

### 6.3. Utility of acoustic monitoring

The intriguing infrasonic signals recorded at Pichincha indicate an activity that is distinct from the Strombolian-type volcanoes presented earlier. Not only is the frequency content of Pichincha infrasound substantially different, but the radical travel time difference between acoustic and seismic phases indicates a substantial amount of pre-eruptive seismicity. Hypocenters determined by the Instituto Geofisico local seismic network indicate that earthquakes may originate as deep as 3 km below the vent. Hence, travel time differences between acoustic and seismic phases exceeding several tens of seconds may reflect the time necessary for gas to breach the surface from an initial rupture source. This would suggest gas mass transfer rates on the order of $10^2$ m/s. Alternatively, the precursory seismicity could indicate dome intrusion where the delayed infrasound onset reflects sloughing of a portion of the dome caused by destabilization.

The general lack of impulsive infrasound and the presence of extended-duration, broad-band signals (several minutes in duration in some cases) indicate a more continuous, less impulsive style of degassing and/or a very weak eruption onset. Explosion sources originating at depth within a conduit appear to radiate significantly less energy into the atmosphere than into the ground (Johnson, 2000). If the Pichincha explosions are initiated by relatively deep fragmentation, this may explain Pichincha's relatively low infrasound amplitudes. In future experiments it will be vital to decrease speculation about the Pichincha degassing source by observing explosions visually as well as infrasonically. In addition, we must deploy multiple seismo–acoustic stations (with portable dataloggers of sufficient dynamic range) so that Pichincha broad-band infrasound signals may be differentiated from wind noise.

## 7. Discussion

Acoustic airwaves generated by volcanic explosions provide an invaluable tool for the study of degassing source processes because atmospheric propagation filters are relatively benign compared to the seismic propagation filters in a heterogeneous volcanic medium. Because earth propagation filters and scattering effects are so severe, seismic waveforms from two different explosion sources may appear relatively similar. Subtle differences in the character of explosive degassing are thus best expressed by infrasonic pressure signals (Fig. 32).

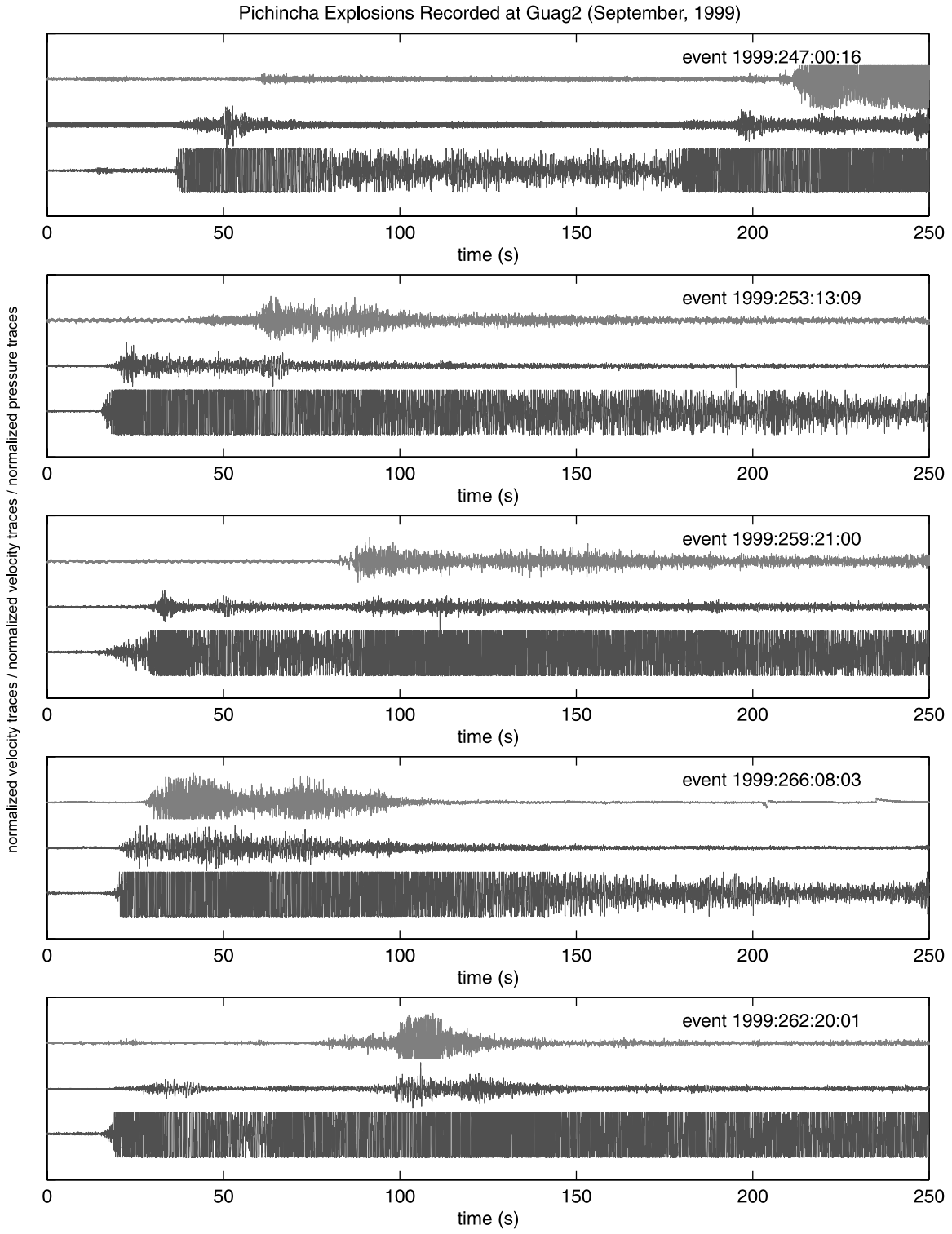
Pichincha Explosions Recorded at Guag2 (September, 1999)
event 1999:247:00:16
event 1999:253:13:09
event 1999:259:21:00
event 1999:266:08:03
event 1999:262:20:01
normalized velocity traces / normalized velocity traces / normalized pressure traces
time (s)
0
50
100
150
200
250

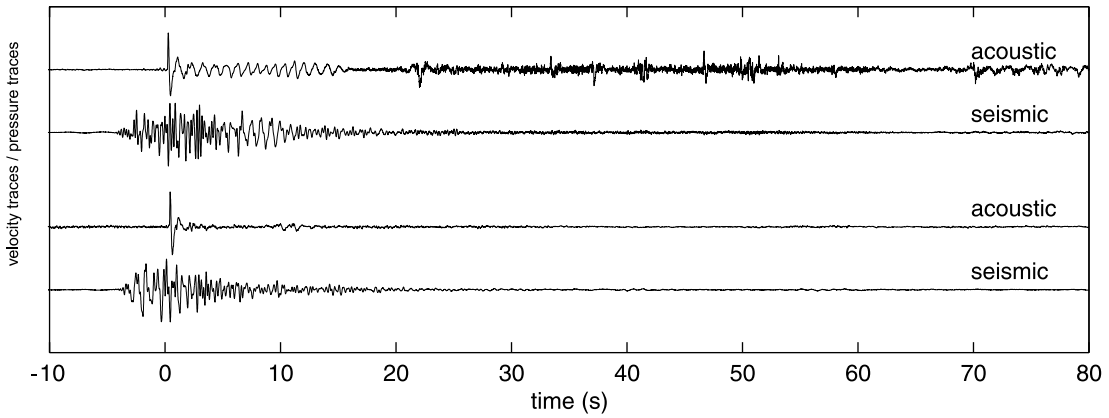


Fig. 32. Explosion signals characterized by infrasound. Two different explosions (1999:251:07:37 and 1999:251:10:15) recorded at Karymsky Volcano. Despite similar seismic envelopes and seismic coda lengths, the associated acoustic signals are quite different.

Researchers at other erupting volcanoes, notably Klyuchevskoi (Firstov and Kravchenko, 1996), Stromboli (Vergniolle et al., 1996), Unzen (Yamasato, 1998), Sakurajima (Garces et al., 1999), and Arenal (Hagerty et al., 2000), have recognized the merits of infrasound as a tool for the understanding of volcanic degassing phenomena at a specific volcano. However, infrasound also provides a special opportunity for the comparison of eruptive activity at different volcanoes because atmospheric pressure records are mostly independent of site-specific propagation effects (for microphones deployed at intermediate distances). A critical evaluation of the seismic signals from explosions at two different volcanoes must take into account variable site responses, instrument responses, background seismic noise, and most importantly volcanic structure and propagation paths. Fig. 33 provides examples of infrasonic pressure traces recorded at the Klyuchevskoi, Stromboli, Unzen, Arenal, and Sakurajima volcanoes for comparison with the infrasonic signals introduced earlier in this paper.

Of all the pressure traces displayed in Fig. 33, Klyuchevskoi and Stromboli infrasound appear the most similar to the explosion signals recorded at Erebus (compare Figs. 4 and 33a,b). The signals recorded at these three sites consist primarily of single, short-duration, quasi-sinusoidal pulses. This type of infrasonic signal may be common at relatively low-viscosity systems. In fact, the basaltic magmas of both Klyuchevskoi and Stromboli probably share similar fluid dynamic properties with the phonolite of Erebus (Dibble et al., 1984). At both Stromboli and Erebus, large bubbles have been observed rising to the surface and bursting and it is probable that the same mechanism occurs at Klyuchevskoi (Firstov and Kravchenko, 1996). Degassing signals which are characterized primarily by a single, short-duration infrasonic pulse probably represent a gas volume rupture from near the surface of an open, low-viscosity fluid body (either a conduit or lava lake). Gas release in this type of environment may occur without an equivalent ejection of degassed magma.

Arenal infrasound can be considered an analog for the infrasound recorded at both Karymsky and Sangay (Figs. 11, 21, and 33d,e). Explosive activity at these three sites is characterized as

Fig. 31. Pichincha explosion examples from Guag2. Five normalized explosions recorded with the McChesney 16-element microphone at station Guag2 (top trace) and with short-period network seismometers at station CGG (bottom two traces). Both the low-gain seismic trace from CGG (middle) and high-gain seismic trace from CGG (bottom) are provided. High gain signals are clipped due to dynamic range limitations of the telemetry.

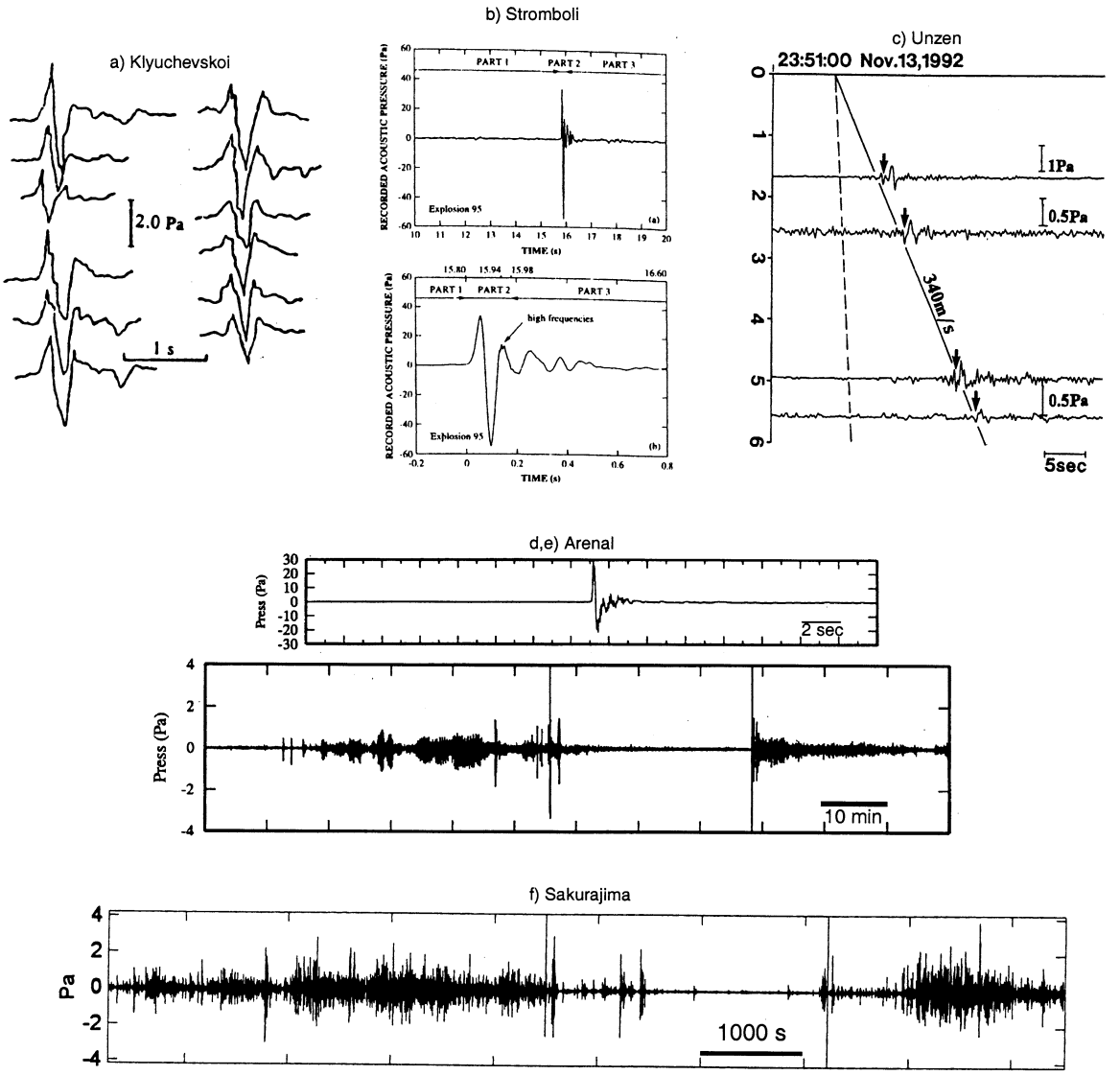


Fig. 33. Infrasonic records from degassing volcanoes. Acoustic records of degassing activity from several volcanoes. Examples are from: (a) Klyuchevskoi (Firstov and Kravchenko, 1996), (b) Stromboli (Vergniolle et al., 1996), (c) Unzen (Yamasato, 1998), (d,e) Arenal (Hagerty et al., 2000), and (f) Sakurajima (Garces et al., 1999).

Strombolian because the eruption consists primarily of discrete explosion events. However, the character of the explosions at these three volcanoes differs fundamentally from low-viscosity Strombolian centers (Stromboli and Erebus), where explosions do not generally possess extended-duration degassing codas. Extended-duration degassing events at Arenal, Karymsky, and Sangay may be attributed to a combination of higher magma viscosity, impediments in the vent/conduit, and/or variable depths of fragmentation (Johnson and Lees, 2000). The magma composition at Arenal, Karymsky, and Sangay is primarily andesitic with considerably higher vis-

cosity than Stromboli basalt or Erebus phonolite. Although Sparks (1997) suggests that andesitic Strombolian conduits possess open vents, low yield-strength caps of rubble may serve to temporarily plug these orifices. Flux of solid material from the vents of Arenal, Karymsky, and Sangay is generally greater than the solid flux at the lower viscosity Strombolian-type volcanoes as evidenced by dirtier eruption plumes, emission of large bombs, and concurrent lava flows (Johnson and Lees, 2000; Hagerty et al., 2000). It may be that degassing at these more viscous, andesitic, Strombolian-type centers can not readily occur without a corresponding flux of exsolved magma.

Sakurajima infrasound and eruptive behavior most closely resembles the infrasonic signals and eruptive behavior from Tungurahua. At both Sakurajima and Tungurahua (Figs. 27 and 33f), infrasound is relatively high-amplitude and quasi-continuous for time intervals exceeding several hours. During the periods of infrasonic monitoring at both Tungurahua and Sakurajima, activity is classified as Vulcanian, characterized by vigorous and nearly continuous emissions of ballistics, ash, and gas (Garces et al., 1999). Average plume heights at both Sakurajima and Tungurahua extend several kilometers above the vent and are substantially more energetic than the average plumes associated with the Strombolian explosions at Arenal, Karymsky, Sangay, Erebus, or Stromboli. A critical comparison between infrasound intensities at Strombolian and Vulcanian sites is an important future study.

Unzen and Pichincha degassing signals are enigmatic due to the infrequence of visual observations of associated degassing. Both volcanoes possess active dacite domes which experience occasional sloughing or collapse, but the exact physical source responsible for the infrasound shown in Figs. 30, 31, and 33c is unclear. Yamasato (1998) believes that Unzen infrasound is produced by gas escaping through cracks in the dome which is a possible mechanism at Pichincha also. The primary similarities between Unzen and Pichincha infrasound are the relative infrequence of explosions and a general lack of high-amplitude impulsive event onsets. In both cases it is often difficult to differentiate low-amplitude degassing signals from background noise. Though the similarities between Unzen and Pichincha infrasound should not be overemphasized, it can be noted that their infrasound differs significantly from the infrasound produced by lower-viscosity Strombolian-type volcanoes.

## 8. Summary and conclusion

The acoustic and seismic signals presented in this paper come from five volcanoes which exhibit frequent, but relatively low-vigor degassing explosions. With the exception of Pichincha Volcano (dacitic composition), the volcanoes each have relatively low silica magmas and low magma viscosities (phonolite – Erebus, andesite – Karymsky, Sangay, and Tungurahua). At the time of our studies, Karymsky, Sangay, and Erebus each produced distinct degassing explosions characteristic of Strombolian-type activity. Tungurahua had a more vigorous and continuous Vulcanian style of degassing. And Pichincha displayed irregular phreato-magmatic or dome-collapse activity. With the exception of Pichincha, the vents at each volcano can be broadly classified as ‘open’.

At each field site electret condenser element microphones with responses in the near-infrasonic bandwidth were co-deployed with seismometers less than 10 km from the degassing sources. At these distances, verification of explosive degassing proved trivial during periods of light wind (less than 2 m/s; see Appendix); however, the deployment of multiple microphones (such as in the arrays at Karymsky and Erebus) greatly improved signal analysis. These arrays allow for the recovery of accurate explosion source overpressures, as well as source locations and origin times. In the future, Sangay, Tungurahua, and Pichincha would each benefit from studies that include the deployment of multiple microphones. It will be equally important to document the degassing signals visually at these sites. Pichincha and other active volcanoes with high-silica, viscous magmas must receive more infrasonic attention in the future because their activity is less well understood than the activity at the Strombolian systems which have been the traditional focus of seismo–

Table A1
Microphone response summary. Instrument sensitivity and high-pass 3 dB point reflect the combined response of pressure sensing element, amplifier, and associated filters determined either in the McChesney laboratory control box (*) or in the field by co-location with the Larson–Davis precision microphone (**). Microphones which are not calibrated by either method have responses listed as unknown.

| Station | Microphone type | Sensitivity | 3 dB |
|---|---|---|---|
| EHUT* | Larson–Davis[a] | 42 mV/Pa | 0.27 Hz** |
| EHUT* | McChesney 4[b] | 200 mV/Pa | 3.0 Hz |
| EHEL* | McChesney 4[b] | 170 mV/Pa | 4.9 Hz |
| ENKB* | McChesney 4[b] | 130 mV/Pa | 1.4 Hz |
| ECON* | McChesney 4[b] | 130 mV/Pa | 4.5 Hz |
| EE1S* | McChesney 4[1b] | 140 mV/Pa | 1.7 Hz |
| EE1S | Dibble[c] | 70 mV/Pa | flat |
| Kar1* | Ramey[d] | 7.8 mV/Pa | flat |
| Kar1 | Ripepe-A[e] | unknown | ? |
| Kry1* | Larson–Davis[a] | 42 mV/Pa? | 0.27 Hz |
| Kry2* | Venema-low[f] | 30 mV/Pa | ~5 Hz |
| Kry3* | Venema-high[f] | 160 mV/Pa | ~4 Hz |
| V1, L1, R1** | Ripepe-B[g] | 320 counts/Pa | ? |
| V2, L2, R2** | Ripepe-B[g] | 310 counts/Pa | ? |
| V3, L3, R3** | Ripepe-B[g] | 80 counts/Pa | ? |
| V4, L4, R4** | Ripepe-B[g] | 210 counts/Pa | ? |
| Krm3* | Larson–Davis[a] | 42 mv/Pa | 0.27 Hz |
| Krm3** | McChesney 1[b] | 50 mv/Pa | ~2.5 Hz |
| Krm3** | McChesney 4[b] | 200 mv/Pa | ~2.5 Hz |
| Krm9** | McChesney 4[b] | 100 mv/Pa | ~2.5 Hz |
| Krm9** | Venema-high[f] | 500 mv/Pa | ? |
| Krm1** | McChesney 4[b] | 100 mv/Pa | ~2.5 Hz |
| Krm2** | McChesney 4[b] | 200 mV/Pa | ~2.5 Hz |
| Krm0** | McChesney 4[b] | 100 mV/Pa | ~2.5 Hz |
| San1* | Venema-low[f] | ~30 mV/Pa | ~5 Hz |
| Tung | McChesney 4[b] | unknown | ~2.5 Hz |
| Guag1 | Venema-low[f] | unknown | ? |
| Guag2 | McChesney 16[b] | unknown? | ? |

[a] The Larson–Davis free-field precision microphone used at the experiments at Karymsky and Erebus is a commercially available electret condenser microphone suitable for engineering purposes. The microphone deployed at Karymsky and Erebus consisted of a one-inch electret condenser element No. 2570, preamp PRM900C, and a power supply 2200C. Specifications are provided by Larson–Davis and verified in the McChesney laboratory calibration box. Laboratory calibration tests reveal a behavior which closely resembles a single-pole high pass filter with corner frequency at 0.27 Hz. In many experiments, the Larson–Davis microphone was temporarily co-deployed with other electret condenser microphones to assess the relative response of the other instruments.

[b] McChesney 1-, 4-, and 16-element microphones consist of a variable gain amplifier, low-pass RC filters (~20 Hz), and 1–16 individual WM-52BM Panasonic omnidirectional condenser elements. Each Panasonic condenser element has a slightly different sensitivity and corner frequency (~1–~5 Hz) which limit their application for infrasonic waveform modeling. However, the spatial wind filtering abilities of the McChesney 4 and 16 boxes allow identification of acoustic pulses in windy conditions (Fig. A6). Of all the McChesney units used in this study, only the microphones deployed at Erebus have undergone careful laboratory calibration tests to determine sensitivity and corner frequency so that instrument responses may be removed. McChesney microphones deployed at Karymksy were calibrated only by temporary co-location with the Larson–Davis microphone. Frequency response of the McChesney microphones resembles a single-pole high-pass filter to first order. Design and construction of the McChesney microphones is by the authors (PNSN, University of Washington).

[c] The Dibble microphone is a pressure transducer microphone that has been continuously operating at Erebus since 1991. The microphone active element is a SenSym LX02002D transducer. Associated electronics have a passband of 0.3–13 Hz. Output from the microphone is telemetered to a data acquisition center in McMurdo. Design, construction, and calibration information is by Raymond Dibble (Victoria University, Wellington, New Zealand).

Table A1 (*Continued*).

[d] The Ramey microphone is a replica of the Dibble microphone that was deployed temporarily at Karymksy in 1997. Pressure sensing element is a SenSym LX06002D transducer. Microphone sensitivity was obtained in laboratory calibration tests in 2000. Frequency response is flat except for a low-pass filter ($\sim$20 Hz) used to remove high-frequency acoustic signals. Construction of microphone is by Jim Ramey (PNSN, University of Washington).

[e] The Ripepe-A microphone contains an electret condenser element, amplifier of unknown gain, and a band-pass filter. It was deployed at Karymsky in 1997. Sensitivity and corner frequencies are not constrained. Design and construction is by Pasquale Poggi (Instituto di Ottica, Florence, Italy).

[f] Venema microphones (low and high gain) use Radio Shack omnidirectional electret condenser elements (270-092B). The attached variable-gain amplifier and low-pass filters ($\sim$20 Hz) were designed and built by Brian Venema (Physics Electronics Shop, University of Washington). This microphone was used at Karymsky, Sangay, and Pichincha. Unfortunately, laboratory calibration tests conducted in 2000 may reflect deterioration of the sensing elements during their long life span. Absolute sensitivity at Pichincha is entirely unknown because signals were conveyed by telemetry at unknown gain.

[g] Ripepe-B microphones consist of a single electret condenser element (unknown manufacturer), amplifier, and low-pass filter. Sensitivity (listed in counts/Pa for the Datamark acquisition system) was determined by temporary co-location of microphones with a Larson–Davis microphone. Microphone circuitry designed and built by Maurizio Ripepe (Instituto di Ottica, Florence, Italy) and Evgenii Gordeev (OMSP, Kamchatka, Russia).

acoustic experiments. Visual observations are much more difficult to achieve at silicic systems because their explosions tend to be infrequent and hazardous.

Infrasonic monitoring of volcanic activity provides an invaluable tool for both scientific analysis and hazard assessment. From a research standpoint, infrasound offers the means to reconstruct gas release from the vent. Unlike volcano seismology, infrasound is a direct measure of the acceleration of gases and is thus a more appropriate tool for constraining degassing source dynamics. In many instances (such as at Tungurahua and Pichincha), infrasound offers the only reliable means to differentiate between sub-surface seismicity and the seismicity associated with explosive degassing. Seismic source motions internal to a volcano provide much useful information about volcanic unrest, but it is ultimately the surficial processes (e.g. the presence or intensity of an eruption) which create volcanic hazards. Though this paper primarily focuses on volcanoes with low objective hazard (such as Erebus and Karymsky), the experiments at these laboratory volcanoes provide a framework for understanding infrasound generation at more explosive systems. Future study of eruption dynamics and future responses to volcanic crises must incorporate low-frequency acoustic monitoring to optimize our understanding of all types of volcanic degassing.

## Acknowledgements

We express our gratitude to our colleagues at the Escuela Politecnica Nacional in Quito, the Russian Academy of Sciences in Petropavlovsk, and those who helped with technical and instrument support from both PASSCAL and the PNSN. Partial support was provided by US Geological Survey Joint Operating Agreement 1434-95-A-1302 and 1434-95-A-1937, the US Antarctic Program, Naval Warfare Center Grant 68936-97-C-0001, and NSF Grants V9W19267, OPP9814921, and EAR-9614639. We acknowledge Charlotte Rowe's thorough review which served to improve this manuscript. Finally, we will never forget the tireless work and overall contributions provided by our good friend Diego Viracucha of the Escuela Politecnica Nacional in Quito.

## Appendix. Microphone specifications and wind noise

The analysis of infrasonic and seismic waveforms must both contend with the same signal processing issues. In each case instrument response must be removed and environmental noise must be minimized. This appendix summarizes the responses of the microphones used in the studies at Erebus, Karymsky, Sangay, Tungurahua,

and Pichincha (Table A1) and describes how transfer functions can be applied to recover the true acoustic pressure time history. This appendix also details background noise levels and wind noise minimization schemes used in some of the experiments.

*Microphone Response*

The pressure sensing elements commonly used in infrasonic studies at volcanoes are either pressure transducers or electret condenser elements. Each of these devices comes with its own set of benefits and drawbacks. Pressure transducers (used in the Dibble and Ramey microphones) are economical and have a flat frequency response down to DC frequencies, but suffer from electronic noise. Electret condenser microphones are somewhat less noisy, but possess a relatively poor response at very low frequencies (below ~1 Hz). The mass-produced condenser elements (used in the McChesney, Ripepe, and Venema microphones) have corner frequencies ranging from 1 to 5 Hz, which provides sufficient bandwidth for the study of much volcanic infrasound. However, these mass-produced electret condenser elements are inferior to more expensive, engineering-quality condenser element microphones (such as the Larson–Davis instrument with corner frequency at approximately 0.25 Hz).

The active elements of both electret condenser elements and pressure transducers operate in a similar manner. Atmospheric pressure waves deflect a diaphragm (usually a metal alloy filament in electret condenser elements, or an etched silicon chip in pressure transducers) which varies the dimension of a capacitive gap. Changes in voltage or current across the gap are analog filtered and amplified by adjoining circuitry, and then digitized to a datalogger or telemetered as a frequency modulated tone. Because the capacitive gap in an electret condenser element is 'leaky', there is a response roll-off at lower frequencies. Pressure transducers, on the other hand, suffer no leakage if operated in an absolute mode, where one side of the diaphragm is permanently sealed. In this scenario, barometric fluctuations (which have pressure variations to the order of $10^3$ Pa) are high-pass filtered before conveyance to a recording device. The main deficiency of absolute pressure transducers is their relatively high electronic noise level compared to electret condenser elements.

Most of the microphones deployed at the five volcanoes discussed in this paper used electret condenser elements because of their heightened sensitivity with respect to a noise floor. Since manufacturers of electret condenser elements do not generally provide frequency response information in the infrasonic bandwidth, we performed our own instrument calibration by constructing a test chamber consisting of a sealed speaker

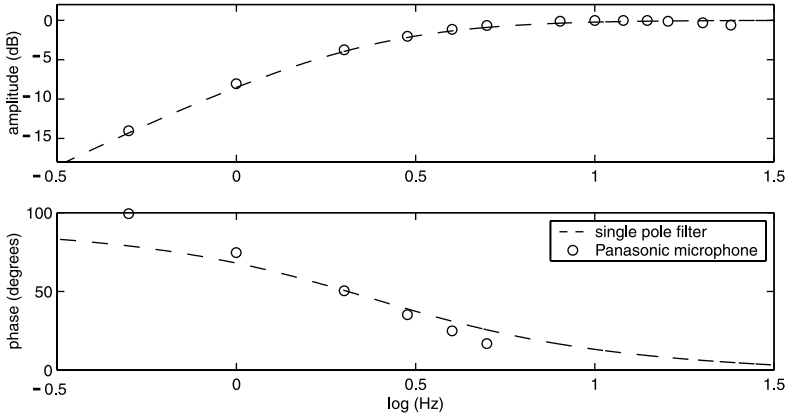


Fig. A1. Frequency response of electret condenser element. Panasonic electret condenser elements used in the McChesney microphones have frequency responses closely resembling a single-pole high-pass filter. The example shows a microphone element with a corner frequency of 2.5 Hz. Corner frequencies for all Panasonic microphones (WM-52BM) lie between 1 and 5 Hz.

box and an inward-facing woofer that could be oscillated sinusoidally at infrasonic frequencies. We placed our field microphones in the control box along with a SenSym SCXL004DN absolute pressure transducer of known sensitivity and frequency response. By varying the frequency of oscillation of the speaker diaphragm, we were able to assess the amplitude and phase response of our electret condenser microphones.

*Transfer function*

Deconvolution of the microphone response is a necessary step for infrasonic waveform modeling. Our laboratory calibration tests provide sufficient frequency and phase information to generate suitable transfer functions for the Larson–Davis and McChesney microphones. Instrument response for these microphones closely resembles a single-pole high-pass filter. Fig. A1 shows an example of the frequency and phase response for a single Panasonic electret condenser element (WM-52BM) used in the McChesney 1-, 4-, and 16-element microphone boxes.

Transfer functions may be easily applied in the frequency domain using seismic signal processing

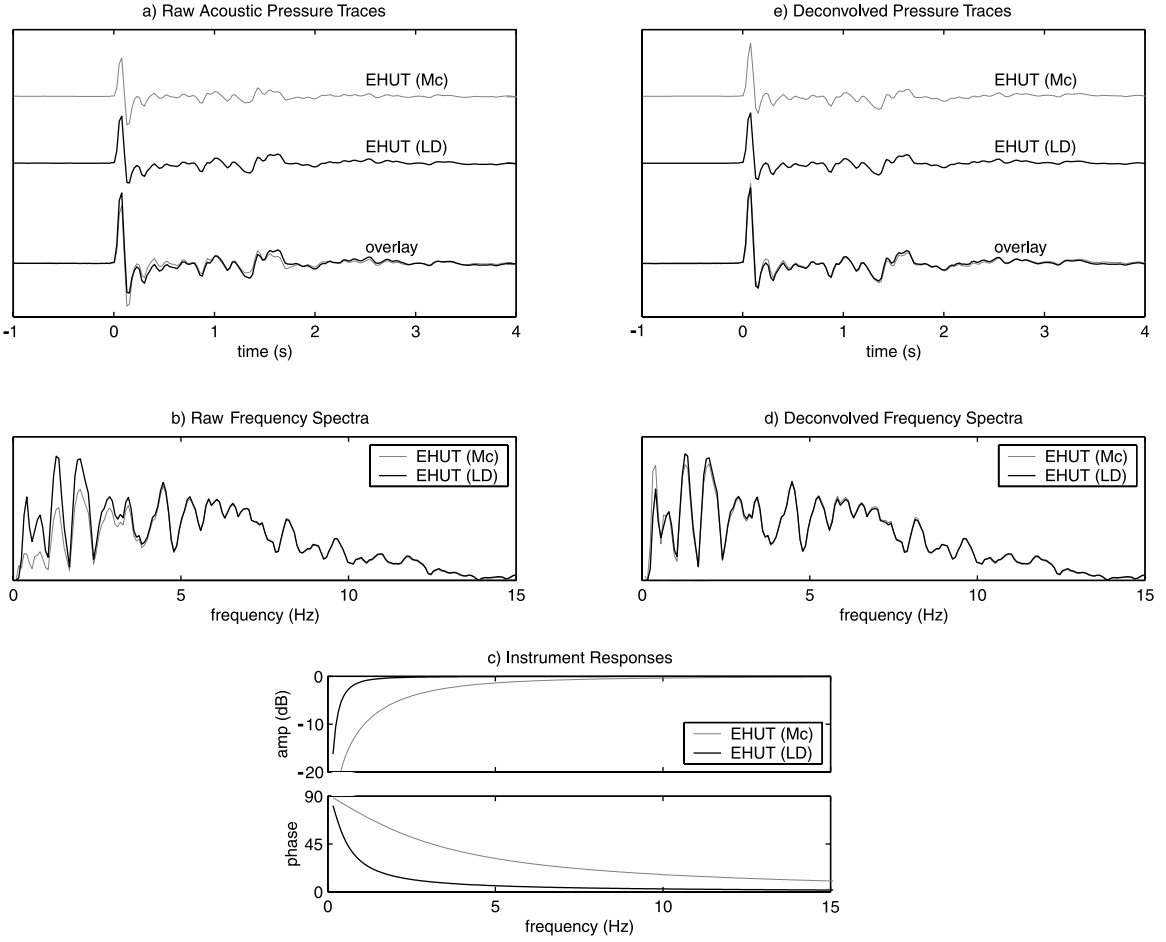


Fig. A2. Deconvolution of microphone response. (a) Unfiltered acoustic pressure traces. (b) Associated frequency responses. (c) Transfer functions for single-pole filters with different corner frequencies. (d) Frequency spectra after removal of instrument response. (e) Deconvolved waveforms.

software. Fig. A2 illustrates instrument deconvolution for both the Larson–Davis and a McChesney 4-microphone. Both instruments were co-located at Erebus at station EHUT. After removal of the instrument response, the similarity of the infrasonic waveforms is greatly improved. By applying the appropriate transfer function, maximum excess pressure increases by about 20% for the McChesney microphone.

*Noise*

Both electronic and environmental noise can be problematic during the analysis of infrasonic signals. Electronic noise level is independent of microphone sensitivity and environmental noise, and depends solely upon the pressure sensing element, associated electronics, and data acquisition system. Though a low-noise op-amp is usually employed to increase effective instrument sensitivity, it also boosts the inherent electronic noise associated with the microphone sensor. In general, electret condenser elements possess lower inherent electronic noise than pressure transducers for identical amplification and data acquisition systems. However, this electronic noise only becomes problematic for pressure transducers deployed in recording situations where environmental and datalogger noise is very low. There was, for instance, no advantage to using electret condenser elements at Pichincha, where noise associated with telemetry and wind was far greater than the noise produced by the pressure sensing components.

In most situations, wind noise is by far the

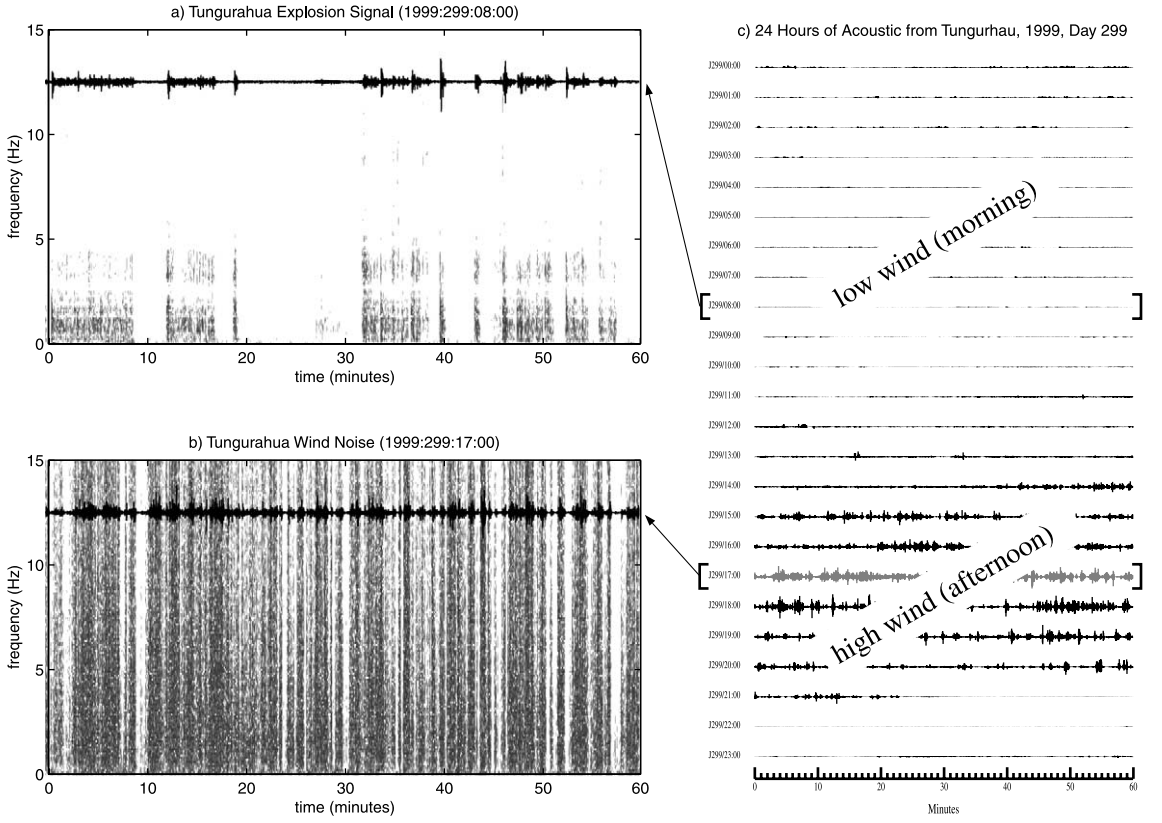


Fig. A3. Tungurahua wind noise. (a) Low-amplitude infrasonic signals associated with explosive degassing have a predominance of low frequencies. (b) In contrast, wind noise is high amplitude and broad-band. (c) 24-h acoustogram at Tungurahua shows the relative amplitudes of wind and signal indicating a tendency for wind noise to cluster in time (generally during the afternoon at Tungurahua).

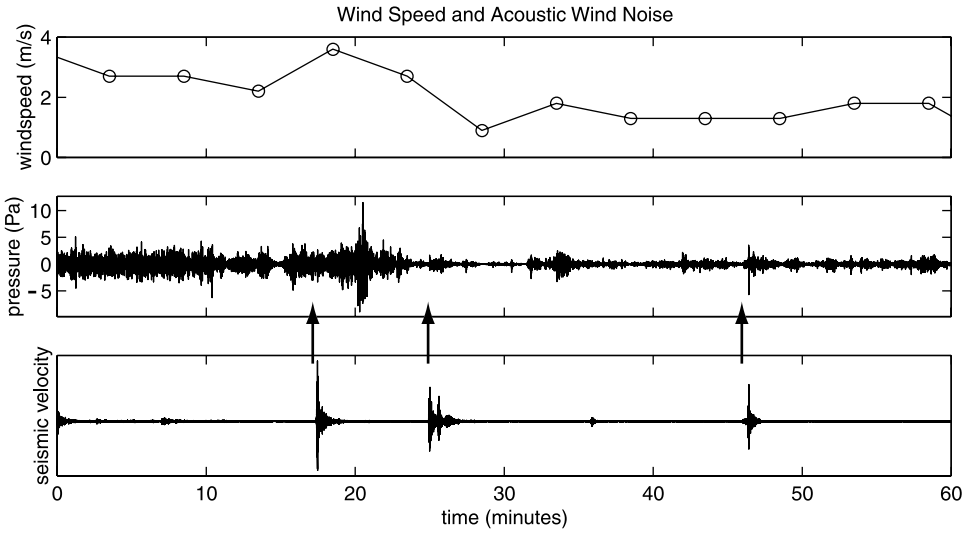


Fig. A4. Wind noise vs. wind speed. The relationship between wind speed and acoustic noise at a microphone deployed at Karymsky (station Krm3). Seismic events (and arrows) correspond to explosions with associated acoustic pulses that are mostly obscured by wind noise (except for the third explosion). Anemometer wind speeds (top plot) are sampled 5 m from the microphone and averaged over 5-min intervals.

most significant source of infrasonic signal corruption. During periods of heavy wind, acoustic signals corresponding to degassing may be completely obscured by this high amplitude 'tremor'. Fig. A3 illustrates acoustic traces associated with both degassing signal and wind noise at Tungurahua Volcano. It is apparent that wind noise can have a much higher amplitude than degassing signals and that it is broad-band (nearly white). Thus it is extremely difficult to remove wind noise during the post-processing of infrasonic data.

Wind noise is well-correlated with wind speed (Fig. A4). For a single electret condenser element, the root-mean-square pressure appears exponentially related to wind speed (Johnson et al., 1999). During field experiments, the best tactic for wind

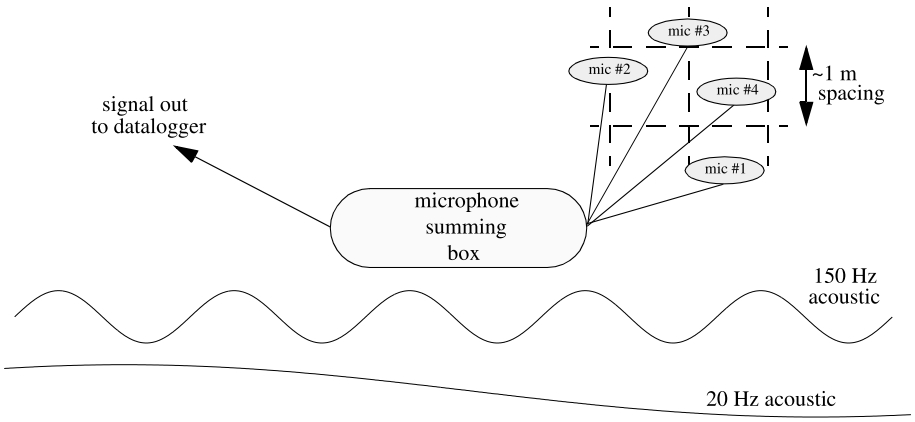


Fig. A5. Multi-element microphone. Scheme showing the design of the McChesney 4-microphone summing box. Meter spacing between individual sensors is sufficient for incoherent wind noise to combine destructively at the different sensors. However, a 20-Hz acoustic signal ($\sim$17 m wavelength) is oblivious to the microphone separation. The summing box contains amplifier and low-pass filter.

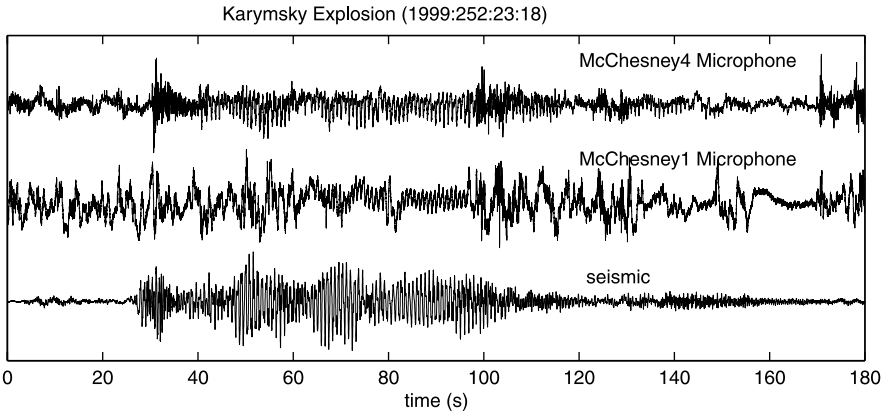


Fig. A6. Wind noise cancellation. Wind noise is a persistent problem on both acoustic channels, but the McChesney 4-microphone shows improvement for the displayed Karymksy explosion signals. The 1-element microphone was co-located with the 4-element microphone which had ~1.5 m sensor spacing. Both microphones were deployed at station Krm3, 1450 m from the vent.

noise minimization is the deployment of microphone sensors away from windy locales. In our experiments we always tried to position our microphones below ridge tops and within a few centimeters of the ground. We also experimented with the placement of sensors in the lee of a wind barrier, but the exact noise reduction benefits are unknown because eddies can be generated by these obstacles. Acoustic sensors buried in snow at Erebus Volcano seemed to produce very good signal-to-noise. Similarly, researchers at Stromboli seem to obtain good results by covering their acoustic sensors with a few centimeters of porous ash (Maurizio Ripepe, pers. commun., 2001). Our calibration studies, involving the co-location of buried and unburied microphones, tend to show minimal infrasound attenuation for snow and some other types of windscreens.

An attempt to filter problematic wind noise resulted in our development of the McChesney 4- and 16-element microphones. These microphones combine input from multiple sensors which are physically separated to spatially filter out incoherent wind noise (Fig. A5). For sensor-spacing less than a few meters, all infrasound is coherently stacked (quarter wavelength at 20 Hz is about 4 m), but wind noise across the small array should be incoherent and combine destructively. Signal-to-noise improvement should theoretically be proportional to the square root of the number of sensors used (Horowitz and Hill, 1989).

For the 4-element McChesney microphone, a 6-dB improvement in signal-to-noise could be expected under optimal conditions. Although a factor of two signal-to-noise gain may be ineffective for recovering degassing signals during periods of extreme wind (such as the noisy trace displayed in Fig. A3b), spatial filtering can be a benefit when wind is moderate. Fig. A6 shows infrasonic explosion signals from Karymsky in 1999 recorded with co-located McChesney1 and McChesney4 microphones. The multi-element microphone appears to record the explosion more cleanly, demonstrating its utility as a wind filter. In certain instances, the reduction in noise may be sufficient to allow for the detection of degassing signal above background wind.

## References

Aki, K., Koyanagi, R., 1981. Deep volcanic tremor and magma ascent mechanism under Kilauea, Hawaii. J. Geophys. Res. 86, 7095–7110.

Benoit, J.P., McNutt, S.R., 1997. New constraints on source processes of volcanic tremor at Arenal Volcano, Costa Rica using broadband seismic data. Geophys. Res. Lett. 24, 449–452.

Brodsky, E.E., Kanamori, H., Sturtevant, B., 1999. A seismically constrained mass discharge rate for the initiation of the May 18, 1980 Mount St. Helens eruption. J. Geophys. Res. 104, 29387–29400.

Dibble, R.R., Kienle, J., Kyle, P.R., Shibuya, K., 1984. Geophysical Studies of Erebus Volcano, Antarctica, from 1974

December to 1982 January. N.Z. J. Geol. Geophys. 27, 425–455.

Dibble, R.R., O'Brien, B., Rowe, C.A., 1994. The velocity structure of Mount Erebus, Antarctica, and its lava lake. In: Kyle, P.R. (Ed.), Volcanological and Environmental Studies of Mount Erebus, Antarctica. Antarctic Research Series 66, American Geophysical Union, Washington, DC, pp. 1–16.

Firstov, P.P., Kravchenko, N.M., 1996. Estimation of the amount of explosive gas released in volcanic eruptions using air waves. Volcanol. Seismol. 17, 547–560.

Garces, M.A., Hagerty, M.T., Schwartz, S.Y., 1998. Magma acoustics and time-varying melt properties at Arenal Volcano, Costa Rica. Geophys. Res. Lett. 25, 2293–2296.

Garces, M.A., Iguchi, M., Ishihara, K., Morrissey, M.Sudo,Y., Tsutsui, T., 1999. Infrasonic precursors to a vulcanian eruption at Sakurajima Volcano, Japan. Geophys. Res. Lett. 26, 2537–2540.

Garces, M.A., McNutt, S.R., 1997. Theory of the airborne sound field generated in a resonant magma conduit. J. Volcanol. Geotherm. Res. 78, 155–178.

Gordeev, E.I., Kasahara, M., Levina, V.I., Miyamachi, H., Chebrov, V.N., 1997. Magma activity at Karymsky Volcano and Academy Nauk Caldera (Kamchatka, Russia) triggers large tectonic (M7.0) event. EOS Transactions, American Geophysical Union, 78(46), Fall meeting Suppl., F442.

Hagerty, M., Schwartz, S.Y., Garces, M., Protti, M., 2000. Analysis of seismic and acoustic observations at Arenal Volcano, Costa Rica, 1995–1997. J. Volcanol. Geotherm. Res. 101, 27–65.

Hall, M.L., 1977. El Volcanismo en el Ecuador. IPGH, Quito, 120 pp.

Hall, M.L., Robin, C., Beate, B., Mothes, P., Monzier, M., 1999. Tungurahua Volcano, Ecuador; structure, eruptive history and hazards. J. Volcanol. Geotherm. Res. 91, 1–21.

Hellweg, M., 2000. Physical models for the source of Lascar's harmonic tremor. J. Volcanol. Geotherm. Res. 101, 183–198.

Horowitz, P., Hill, W., 1989. The Art of Electronics. Cambridge University Press, New York, 1125 pp.

Johnson, J.B., in press. Generation and propagation of infrasonic airwaves from volcanic explosions. J. Volcanol. Geotherm. Res., this issue S0377-0273(02)00408-0.

Johnson, J.B., 2000. Interpretation of Infrasound Generated by Erupting Volcanoes and Seismo–acoustic Energy Partitioning During Strombolian Explosions. Ph.D. Thesis, University of Washington, Seattle.

Johnson, J.B., Lees, J.M., 2000. Plugs and chugs – Seismic and acoustic observations of degassing explosions at Karymsky, Russia and Sangay, Ecuador. J. Volcanol. Geotherm. Res. 101, 67–82.

Johnson, J.B., Lees, J.M., Gordeev, E.I., 1998. Degassing explosions at Karymsky Volcano, Kamchatka. Geophys. Res. Lett. 25, 3999–4042.

Johnson, J.B., Ruiz, M.C., McChesney, P., 1999. Low-frequency acoustic monitoring and wind-filtering at active volcanoes. EOS Transactions, American Geophysical Union, 80(46), Fall meeting Suppl., F1148.

Julian, B.R., 1994. Volcanic tremor: Nonlinear excitation by fluid flow. J. Geophys. Res. 99, 11859–11877.

Kanamori, H., Given, J.W., 1982. Analysis of long-period seismic waves excited by the May 18, 1980, eruption of Mount St. Helens; A terrestrial monopole? J. Geophys. Res. 87, 5422–5432.

Kyle, P.R., Dibble, R.R., Giggenbach, W.F., Keys, J., 1982. Volcanic activity associated with the anorthoclase phonolite lava lake, Mount Erebus, Antarctica. In: Craddock, C. (Ed.), Antarctic Geoscience. University of Wisconsin Press, Madison, pp. 734–745.

Lees, J.M., Bolton, E.W., 1998. Pressure cookers as volcano analogues. EOS Transactions, American Geophysical Union, 79(45), Fall meeting Suppl., F620.

Monzier, M., Robin, C., Samaniego, P., Hall, M.L., Cotten, J., Mothes, P., Arnaud, N., 1999. Sangay Volcano, Ecuador; Structural development, present activity and petrology. J. Volcanol. Geotherm. Res. 90, 49–79.

Mori, J., Patia, H., McKee, C., Itikarai, I., Lowenstein, P., De Saint Ours, P., Talai, B., 1989. Seismicity associated with eruptive activity at Langila Volcano, Papua New Guinea. J. Volcanol. Geotherm. Res. 38, 243–255.

Rowe, C.A., Aster, R.C., Kyle, P.R., Dibble, R.R., Schlue, J.W., 2000. Seismic and acoustic observations at Mount Erebus Volcano, Ross Island, Antarctica, 1994–1998. J. Volcanol. Geotherm. Res. 101, 105–128.

Ruiz, M., Barba, D., Johnson, J., Seidl, D., 2001. Senales Sismo-acusticas del Volcan Tungurahua. In: Memorias IV Jornadas de Ciencias de la Tierra. Escuela Politecnica Nacional, Ecuador, pp. 81–83.

Ruiz, M., Hall, M., Samaniego, P., Ruiz, G., Villagomez, D., 1999. Seismic activity at Tungurahua Volcano: Correlation between tremor and precipitation rates. Expanded Abstracts, Fourth International Symposium on Andean Geodynamics. IRD, pp. 636–639.

Schlindwein, V., Wassermann, J., Scherbaum, F., 1995. Spectral analysis of harmonic tremor signals at Mt. Semeru Volcano, Indonesia. Geophys. Res. Lett. 22, 1685–1688.

Sparks, R.S.J., 1997. Volcanic Plumes. Wiley, New York, 574 pp.

Vergniolle, S., Brandeis, G., Mareschal, J.-C., 1996. Strombolian explosions, 2. Eruption dynamics determined from acoustic measurements. J. Geophys. Res. 101, 20449–20466.

Yamasato, H., 1998. Nature of infrasonic pulse accompanying low frequency earthquake at Unzen Volcano, Japan. Bull. Volcanol. Soc. Jpn. 43, 1–13.